The histone methyltransferase DOT1L prevents antigen-independent differentiation and safeguards epigenetic identity of CD8$^+$ T cells

Eliza Mari Kwesi-Maliepaard[1]*, Muhammad Assad Aslam[2,3]*, Mir Farshid Alemdehy[2]*, Teun van den Brand[4], Chelsea McLean[1], Hanneke Vlaming[1], Tibor van Welsem[1], Tessy Korthout[1], Cesare Lancini[1], Sjoerd Hendriks[1], Tomasz Ahrends[5], Dieke van Dinther[6], Joke M.M. den Haan[6], Jannie Borst[5], Elzo de Wit[4], Fred van Leeuwen[1,7,#], and Heinz Jacobs[2,#]

[1]Division of Gene Regulation, Netherlands Cancer Institute, 1066CX Amsterdam, The Netherlands

[2]Division of Tumor Biology & Immunology, Netherlands Cancer Institute, 1066CX Amsterdam, The Netherlands

[3]Institute of Molecular Biology and Biotechnology, Bahauddin Zakariya University, 60800 Multan, Pakistan

[4]Division of Gene Regulation, Netherlands Cancer Institute, 1066CX Amsterdam, and Oncode Institute, The Netherlands

[5]Division of Tumor Biology & Immunology, Netherlands Cancer Institute, 1066CX Amsterdam, and Oncode Institute, The Netherlands

[6]Department of Molecular Cell Biology and Immunology, Amsterdam UMC, Location VUmc, 1081HV Amsterdam, The Netherlands

[7]Department of Medical Biology, Amsterdam UMC, location AMC, UvA, 1105 AZ Amsterdam, The Netherlands

* These authors contributed equally to this work.

# Equal contribution and corresponding authors

fred.v.leeuwen@nki.nl; h.jacobs@nki.nl

Lead contact: Fred van Leeuwen

Abstract

Cytotoxic T-cell differentiation is guided by epigenome adaptations but how epigenetic mechanisms control lymphocyte development has not been well defined. Here we show that the histone methyltransferase DOT1L, which marks the nucleosome core on active genes, safeguards normal differentiation of $CD8^+$ T cells. T-cell specific ablation of *Dot1L* resulted in loss of naïve $CD8^+$ T cells and premature differentiation towards a memory-like state, independent of antigen exposure and in a cell-intrinsic manner. Without DOT1L, the memory-like $CD8^+$ cells fail to acquire full effector functions *in vitro* and *in vivo*. Mechanistically, DOT1L controlled T-cell differentiation and function by ensuring normal T-cell receptor density and signaling, and by maintaining epigenetic identity, in part by indirectly supporting the repression of developmentally-regulated genes. Through our study DOT1L is emerging as a central player in physiology of $CD8^+$ T cells, acting as a barrier to prevent premature differentiation and supporting the licensing of the full effector potential of cytotoxic T cells.

Keywords: T cell; Epigenetics; DOT1L; H3K79me2; CD8 memory; virtual memory; innate memory

Running title: Epigenetic control of T-cell fate by DOT1L

Introduction

Lymphocyte development and differentiation is tightly regulated and provides the basis for a functional adaptive immune system. Development of mature T cells initiates in the thymus with progenitor T cells that have to pass two key checkpoints: T cell receptor (TCR) β selection and positive selection, both of which are controlled by intricate signaling pathways involving the pre-TCR/CD3 and αβTCR/CD3 complexes, respectively [1]. Upon positive selection, mature thymocytes are licensed to emigrate and populate peripheral lymphatic organs as naïve T cells (T_N). Further differentiation of naïve T cells into effector or memory T cells normally depends on TCR-mediated antigen recognition and stimulation. However, it has become evident that a substantial fraction of mature $CD8^+$ T cells acquires memory-like features independent of exposure to foreign antigen. The origin and functionality of these unconventional memory cells in mice and humans, also referred to as innate or virtual memory cells, are only just being uncovered [2, 3, 4].

The dynamic changes during development and differentiation of $CD8^+$ T cells are governed by transcriptional and epigenetic changes, including histone modifications that are controlled by chromatin modifiers. Well-established histone marks are mono- and tri-methylation of histone H3K4 at enhancers (H3K4me1) and promoters (H3K4me3), H3K27me3 at repressed promoters, and H3K9me2/3 in heterochromatin [5, 6, 7, 8, 9, 10]. Although epigenetic 'programming' is known to play a key role in T cell development and differentiation, the causal role of epigenetic modulators in T cell differentiation is still poorly understood, especially for chromatin modifiers associated with active chromatin [5].

One of the histone modifications positively associated with gene activity is mono-, di- and tri-methylation of histone H3K79 mediated by DOT1L. This evolutionarily conserved histone

methyltransferase methylates H3K79 in transcribed promoter-proximal regions of active genes [11, 12]. Although the association with gene activity is strong, how H3K79 methylation affects transcription is still unclear and repressive functions have also been proposed [13, 14, 15, 16, 17, 18]. DOT1L has been linked to several critical cellular functions, including embryonic development, DNA damage response, and meiotic checkpoint control [19, 20] and DOT1L has also been shown to function as a barrier for cellular reprogramming in generating induced pluripotent stem cells [21]. DOT1L gained wide attention as a specific drug target in the treatment of MLL-rearranged leukemia, where MLL fusion proteins aberrantly recruit DOT1L to MLL target genes leading to their enhanced expression [22, 23, 24]. A similar dependency on DOT1L activity and sensitivity to DOT1L inhibitors was recently observed in thymic lymphoma [25]. Interestingly, inhibition of DOT1L activity in human T cells attenuates graft-versus-host disease in adoptive cell transfer models [26] and it regulates $CD4^+$ T cell differentiation [27].

Given the emerging role of DOT1L in epigenetic reprogramming and T-cell malignancies, we investigated the role of DOT1L in normal T cell physiology using a mouse model in which *Dot1L* was selectively deleted in the T cell lineage. Our results suggest a model in which DOT1L plays a central role in $CD8^+$ T cell differentiation, acting as a barrier to prevent premature antigen-independent differentiation, and promoting the licensing of the full effector potential by maintaining epigenetic integrity.

Results

DOT1L prohibits premature differentiation of naïve towards memory-like CD8$^+$ T cells

Given the essential role of DOT1L in embryonic development [28], we determined the role of DOT1L in T cell development and differentiation by employing a conditional knock-out mouse model in which *Dot1L* is deleted in the T-cell lineage by combining floxed *Dot1L* with a Cre-recombinase under the control of the Lck promoter, which leads to deletion of exon 2 of *Dot1L* during early thymocyte development (Sup Fig. 1a) [25]. The observed global loss of H3K79me2 in *Lck*-Cre$^{+/-}$;*Dot1L*$^{fl/fl}$ mice, as confirmed by immunohistochemistry on fixed thymus tissue (Sup Fig. 1b), agreed with the notion that DOT1L is the sole methyltransferase for H3K79 [11, 25, 28, 29].

To validate the efficacy of *Dot1L* deletion at the single-cell level, we developed an intracellular staining protocol for H3K79me2. Histone dilution by replication-dependent and -independent means has been suggested to be the main mechanisms of losing methylated H3K79 [15, 30, 31, 32]. Flow-cytometric analyses of thymocyte subsets from *Lck*-Cre$^{+/-}$;*Dot1L*$^{fl/fl}$ mice (hereafter, KO) revealed that double-negative (DN, CD4$^-$CD8$^-$) thymocytes started losing H3K79me2. From the subsequent immature single positive state (ISP) onward all the thymocytes had lost DOT1L mediated H3K79me (Sup Fig. 1c). This confirmed that upon early deletion of *Dot1L*, successive rounds of replication in the thymus allowed for loss of methylated H3K79.

No changes in H3K79 methylation levels were found in T-lineage cells of *Lck*-Cre$^{+/-}$;*Dot1L*$^{wt/wt}$ control mice (hereafter, WT). Ablation of *Dot1L* did not significantly affect the overall thymic cellularity, however it led to a reduction in the number of mature single positive (SP) CD4$^+$ and CD8$^+$ thymocytes

(both 2.5-fold) while the ISP and $CD4^+CD8^+$ double positive (DP) subsets were not significantly affected, suggesting a role of DOT1L in controlling intrathymic T cell selection (Sup Fig. 1d-e).

In the spleen, overall cellularity was also not affected but within the T cell compartment, $CD4^+$ T cells were drastically reduced (3.2-fold), whereas $CD8^+$ T cells were increased (1.7-fold) in number (Sup Fig. 1e-f). However, while flow cytometry of H3K79me2-stained splenic T cells confirmed the lack of DOT1L activity in $CD8^+$ T cells and $CD44^-CD62L^+$ $CD4^+$ T cells, $CD44^+CD62L^-$ $CD4^+$ cells showed a partial loss of H3K79me2 and $CD4^+CD25^+$ regulatory T cells (Treg) remained H3K79me2 positive (Sup Fig. 1g). Since earlier in development, CD4-expressing cells in the thymus were mostly H3K79me2 negative, this suggests that a strong selection occurred for the maintenance of DOT1L for the development of Tregs in this mouse model. Indeed, partial deletion of *Dot1L* in $CD4^+$ cells was confirmed by PCR analysis (Sup Fig. 1h). Here, we focused our study on defining the role of DOT1L in the cytotoxic T cell compartment in which efficient deletion of *Dot1L* and loss of H3K79me2 was found in both the thymus and the periphery.

$CD8^+$ T cell differentiation was strongly affected by the absence of DOT1L. Analysis of $CD8^+$ T cell subsets in the spleen revealed that *Dot1L*-KO mice showed a severe loss of naïve ($CD44^-CD62L^+$) $CD8^+$ T (T_N) cells which was linked to a massive gain of the $CD44^+CD62L^+$ phenotype, a feature of central memory T cells (T_{CM}; Fig. 1A-B*). Lck*-Cre$^{+/-}$*;Dot1L*$^{fl/wt}$ heterozygous knock-out mice (Het) did not show any phenotypic differences of $CD8^+$ T cells (Fig. 1A-B). The lack of haplo-insufficiency was further confirmed by principal component analysis of RNA-Seq data indicating that WT and Het $CD8^+$ T cells clustered together but were separated from the KO $CD8^+$ T cells, excluding gene-dosage effects (Sup Fig. 1i). Therefore, we restricted our further studies to the comparison of the KO and WT mice. The strong shift towards a $CD8^+$

memory-phenotype in *Dot1L* KO was unexpected because *Dot1L*-KO mice were housed under the same conditions as their WT controls and the mice had not been specifically immunologically challenged.

To unravel the molecular identity of the $CD44^+CD62L^+$ *Dot1L*-KO cells in more detail we performed RNA-Seq analysis on sorted $CD44^-CD62L^+$ (T_N) and $CD44^+CD62L^+$ (T_{CM}) $CD8^+$ T cell subsets from WT and KO mice. Based on differential gene expression between T_N and T_{CM} $CD8^+$ cells from WT mice, naïve and memory gene signatures were defined. Interestingly, overlay of these signatures on WT $CD44^-CD62L^+$ (T_N) and KO $CD44^+CD62L^+$ (T_{CM}) cells showed that differential expression between T_N and T_{CM} cells was mostly conserved when *Dot1L* was ablated. (Fig. 1c), although there was misregulation of other genes as well (see below). These data suggest that in the absence of DOT1L, $CD8^+$ T cells cannot retain the naïve identity but rather acquire, prematurely and in the absence of any overt immunological challenge, a transcriptome of memory-like $CD8^+$ T cells.

Dot1L KO memory-like cells are antigen inexperienced

Although WT and KO mice were exposed to the same environment it cannot be excluded that KO mice responded differentially to antigens in the environment. If this is the case one expects skewing in the clonality of the TCRβ gene usage. In order to investigate this possibility, we examined the TCRβ repertoire. *Tcrb*-sequencing revealed no difference in productive clonality scores between WT and KO $CD8^+$ T cells (Sup Fig. 2a). Also, CDR3 length as well as *Tcrb-V* and *Tcrb-J* gene usage were unaffected (Sup Fig. 2b-d). These data, together with the nearly complete loss of naïve $CD8^+$ T cells, argued against any antigen-mediated bias in the selection for $CD8^+$ T cells and indicated that $CD44^+CD62L^+$ memory-like $CD8^+$ T cells in KO mice were polyclonal and arose by antigen-independent differentiation of T_N cells.

Antigen-independently differentiated memory-like $CD8^+$ T cells have already been described in the literature and their origins and functions are subject of ongoing studies [2, 3, 4, 33]. Depending on their origin and cytokine dependency they are referred to as 'virtual' or 'innate' memory cells. Virtual memory $CD8^+$ T cells have been suggested to arise in the periphery from cells that are $CD5^{high}$, related to high TCR affinity, and require IL-15 [4, 34]. In contrast, innate memory $CD8^+$ T cells develop in the thymus and their generation and survival are generally considered to be dependent on IL-4 signaling [3]. We here collectively refer to them as Antigen-Independent Memory-like $CD8^+$ T cells (T_{AIM}). A common feature of these T_{AIM} cells is reduced expression of CD49d [35], a marker that is normally upregulated after antigen exposure. In addition, they express high levels of T-bet and EOMES, encoding two memory/effector transcription factors [36, 37]. In both *Dot1L*-KO and WT, the majority of the $CD44^+CD62L^+$ (T_{CM}) cells were CD49d negative. As a control, $CD44^+CD62L^-$ effector T cells (T_{EFF}) from WT mice challenged with *Listeria monocytogenes* were mostly CD49d positive (Fig. 1d). This further indicates that the generation of $CD44^+CD62L^+$ memory-like T cells in KO mice is independent of antigen exposure. Of note, the percentage of CD49d-negative $CD44^+CD62L^+$ cells that we observed in WT mice corresponds to the percentage of T_{AIM} cells reported in WT B6 mice [38]. Regarding the expression of T-bet and EOMES, most of the KO $CD8^+$ T cells co-expressed T-bet and EOMES. Furthermore, EOMES was expressed at a higher level in KO $CD8^+$ T cells as compared to their WT counterpart (Fig. 1e-f). Together these characteristics are all in agreement with antigen-independent differentiation of naïve $CD8^+$-T cells in the absence of DOT1L.

The T_{AIM} phenotype in *Dot1L* KO initiates in the thymus and is cell-intrinsic

To determine whether peripheral T_{AIM} cells observed in the *Dot1L*-KO setting originate intrathymically, as reported previously for IL-4 dependent innate memory T cells [3], we compared RNA-Seq data from SP $CD8^+$ thymocytes from KO and WT mice. Analyzing the relative distribution of memory and naïve

signature genes revealed that memory genes were among the genes upregulated in KO SP CD8$^+$ thymocytes (Fig. 2a). Importantly, like in peripheral CD8$^+$ T cells the expression of *T-bet* and *Eomes* was highly upregulated in KO SP CD8$^+$ thymocytes. This transcriptional upregulation was corroborated by flow cytometric analysis of protein expression. Intracellular staining for the transcription factors showed that a small but substantial subset of the SP CD8$^+$ KO thymocytes expressed T-bet and EOMES at the protein level (Fig. 2b-c). Together with the unperturbed TCRβ repertoire, this further supports the notion that differentiation of *Dot1L*-KO CD8$^+$ T cells towards memory-like cells initiates intrathymically in an antigen-independent manner. Innate memory cells have been suggested to arise in the thymus in response to an increase in IL-4 producing PLZF^{high} invariant NKT (iNKT) cells or γδ T cells [3]. However, iNKT cells were nearly absent in the thymus of *Dot1L*-KO mice (Fig. 2d-e). Furthermore, the number of γδ T cells did not differ significantly between WT and KO mice (Fig. 2f). Previous studies on innate memory T cells from different mouse models demonstrated that introduction of a transgenic TCR, inhibiting the generation of iNKT and γδ T cells, prevents the development of innate memory cells [39, 40]. However, introduction of the transgenic OT-I TCR, a condition under which the number of iNKT and γδ T cells is strongly reduced [41, 42], did not affect the memory-phenotype of *Dot1L*-KO CD8$^+$ T cells (Fig. 2g). Together, these findings indicate that the intrathymic differentiation of T_{AIM} CD8$^+$ cells in the absence of DOT1L did not depend on an excess of IL4-producing cells in the thymic microenvironment as reported for innate memory T cells. Rather the formation of T_{AIM} cells in *Dot1L*-KO mice likely relates to a cell-intrinsic mechanism.

Dot1L ablation impairs TCR/CD3 expression

One of the cell-intrinsic mechanisms reported to be involved in the formation of T_{AIM} cells is aberrant TCR signaling [2, 34, 43, 44]. Furthermore, treatment of human T cells with DOT1L inhibitor impaired TCR sensitivity and attenuated low avidity T cell responses [26]. This led us to investigate the expression of

genes encoding TCR signaling components in the absence of DOT1L. RNA-Seq analyses confirmed that many TCR signaling genes were differentially expressed between WT and KO SP CD8$^+$ thymocytes (Fig. 3a). Importantly, CD3ζ (CD247), a critical rate limiting factor in controlling the transport of fully assembled TCR/CD3 complexes to the cell surface, was downregulated in *Dot1L*-KO T cells [1, 45, 46, 47, 48]. In addition, other components of the TCR/CD3 complex like CD3e and its associated co-receptor CD8a/b were also downregulated in KO T cells. H3K79me2 ChIP-Seq showed that these genes had H3K79me2 in WT mice and might therefore be directly regulated by DOT1L (Sup Fig. 3a-c). As a consequence, one expects TCR/CD3 and CD8αβ to be reduced at the cell surface of T_{AIM} cells, which we confirmed by flow cytometry (Fig. 3b). In addition to the CD3/TCR complex, we observed downregulation of *Itk*, a key TCR signaling molecule reported to be involved in innate memory CD8$^+$ T cell formation [49]. To exclude that the impaired TCR signaling in KO T cells could be compensated for by the selection of thymocytes expressing TCRs with altered affinity, we kept the TCR affinity identical by crossing the OT-I TCR transgene into our system. Thymocytes expressing OT-I are positively selected in the presence of MHC class I (H-2K^b), mainly generating CD8$^+$ SP T cells expressing the exogenous OT-I TCR, with concomitant reduction of the CD4$^+$ lineage [50]. If DOT1Ldeficiency impairs TCR surface density and signaling, positive selection of conventional OT-I CD8 thymocytes is expected to be compromised. In *Dot1L*-KO mice expressing OT-I, the number of SP CD8$^+$ thymocytes was decreased (3.8-fold) compared to WT mice expressing OT-I (Fig. 3c). This revealed that like with endogenous TCR, early intrathymic ablation of *Dot1L* in the T cell lineage prohibits positive section of conventional OT-I CD8$^+$ T cells, but yet supports the generation and selection of T_{AIM} cells (Fig. 2g) of which the vast majority expressed both exogenous TCR chains (TCRαV2 and TCRβV5) (Fig. 3d). Consistent with the low surface expression of TCR/CD3 and CD8 in the KO condition, the surface expression of OT-I TCR was also lower, as determined by SIINFEKL/H-2K^b tetramer staining (Sup Fig. 3d). This was further validated by staining with antibodies for the transgenic TCR chains TCRαV2 and TCRβV5 which indicated two-fold reduction in KO (Fig. 3b and d).

The TCRαV2 element of the OT-I TCR was under the control of an exogenous promoter, suggesting that the reduced surface expression of OT-I TCR on KO T cells did not relate to transcriptional silencing of native TCR gene promoters. Instead, the observed lower TCR surface levels in KO T cells likely relate to the reduced CD3ζ expression [48]. In conclusion, DOT1L regulates the levels of TCR complex and signaling molecules independent of the selected TCR. In the absence of these regulatory mechanisms, the identity of naïve $CD8^+$ T cells cannot be maintained, contributing to premature T cell differentiation.

Dot1L-KO T_{AIM} cells display memory features but are functionally impaired _in vitro_

A hallmark of memory T cells is that they proliferate faster and produce IFNγ rapidly upon stimulation compared to naïve T cells [51]. Likewise, innate and virtual memory T cells rapidly produce IFNγ upon TCR stimulation [38, 44]. To determine the proliferative potential of *Dot1L*-KO T_{AIM} cells, we activated B-cell depleted, CFSE-labeled splenocytes *in vitro* with anti-CD3 and anti-CD28 antibodies. Proliferation was determined by CFSE dilution. *Dot1L*-KO $CD8^+$ T cells proliferated faster than WT cells (Fig. 4a). In addition, they rapidly became activated $CD44^+CD62L^-$ (Sup Fig. 4a). However, in contrast to WT, KO $CD8^+$ T cells failed to produce IFNγ (Fig. 4b and Sup Fig. 4b), and expressed lower levels of CD69, a marker of activation (Sup Fig. 4c). This indicates a functional impairment of *Dot1L*-KO T cells. To test their intrinsic competence to produce IFNγ, *Dot1L*-KO T cells were stimulated in a TCR-independent manner with PMA and Ionomycin. Intracellular staining for IFNγ revealed that the percentage of stimulated $CD8^+$ T cells producing IFNγ was 1.9-fold higher in KO as compared to WT (Sup Fig. 4d). This suggests that *Dot1L*-KO $CD8^+$ T cells only partially respond to TCR stimulation, but that they have the intrinsic capacity to produce IFNγ. The responders in the WT population likely include the naturally existing virtual memory population (Fig. 1). Taken together, *Dot1L* KO T_{AIM} cells displayed some memory-associated features but simultaneously are functionally impaired.

DOT1L is essential for mounting an effective immune response *in vivo*

To determine the *in vivo* immune responsiveness of *Dot1L*-KO T cells, mice were challenged with a sub-lethal dose of *Listeria monocytogenes*. The immune response was monitored in the blood at day -3, 4 and 7 post injection (Fig. 4c). Already at day 4 most $CD8^+$ T cells in the blood had differentiated towards an effector-phenotype ($CD44^+CD62L^-$) in KO mice (Fig. 4d), which is in line with the *in vitro* stimulation data. However, in accordance with the peak of a normal immune response initiated from naïve T cells [52], the peak of activated effectors in WT mice was reached only after seven days. At day 3 and day 7 post injection, mice were sacrificed and spleen and liver were used to determine clearance of the *Listeria* by counting colony-forming units. Despite the fact that in KO at day 3 most T_{AIM} cells had differentiated into activated T cells, the *Listeria* infection was not cleared. At day 7 complete clearance was observed in the spleen from WT-mice, which is in accordance with literature [52]; however, the *Dot1L* KO mice failed to clear *Listeria* (Fig. 4e-f). In order to investigate the reason for the compromised clearance in KO, despite the rapid T_{EFF} formation in the blood upon infection, we examined the splenic $CD8^+$ T cells subsets in more detail. In WT mice the peak of activated ($CD44^+CD62L^-$) $CD8^+$ T cells was at day 7, whereas in *Dot1L* KO mice this was at day 3 (Fig. 4g-h and Sup Fig. 4e). However, the absolute numbers of total $CD8^+$ T cells in KO on day 3 were not higher than in WT. Furthermore, in WT the number of $CD8^+$ T cells at day 7 had increased 8.6-fold, whereas in KO this was only 4.9-fold, suggesting a lack of expansion despite the acquisition of an effector phenotype (Fig. 4i). Indeed, staining for Ki67, a marker of proliferation showed that at day 3, the frequency of $Ki67^+$ $CD44^+CD62L^-CD8^+$ T cells was not increased in KO cells compared to WT (Fig. 4j). Besides the reduced proliferative capacity *in vivo*, even up to day 7, the KO $CD44^+CD62L^-$ $CD8^+$ T cells showed impaired induction of the effector hallmarks KLRG1, IFNγ and CD49d (Fig. 4k-l, Sup Fig. 4f). Together these data indicate that upon *in vivo* challenge with *Listeria monocytogenes*, compromised clearance in KO mice relates to a reduced capacity to proliferate and terminally

differentiate. In conclusion, DOT1L is essential in controlling the proliferation and effector function of T cells.

DOT1L is required for maintenance of epigenetic integrity of CD8$^+$ T cells

In order to mechanistically understand the functional impairment of *Dot1L*-KO CD8$^+$ T_{AIM} cells *in vivo* and how this relates to the epigenome, we performed H3K79me2 ChIP-Seq on sorted CD8$^+$ T cell populations and compared it to the RNA-Seq data. RNA-Seq analyses from CD44$^-$CD62L$^+$ (T_N) and CD44$^+$CD62L$^+$ (T_{CM}) cells revealed that genes that were upregulated in *Dot1L* KO were biased towards being lowly expressed, whereas downregulated genes tended to have higher expression level (Fig. 5a, left panel). To assess how the transcriptome changes in T cells and the transcriptional bias are related to the chromatin-modifying function of DOT1L, we compared the level of H3K79me2 at the 5' end of genes in WT cells with the mRNA expression changes caused by the loss of DOT1L. H3K79me2 was enriched from the transcription start site into the first internal intron of transcribed genes (Sup Fig. 5a), as reported for human cells [53]. Further analysis showed that most of the lowly-expressed genes upregulated in *Dot1L* KO contained no or very low H3K79me2 in WT cells (Fig. 5a right panel and Sup Fig. 5b). Therefore, these genes were not direct targets of DOT1L and are likely to be indirectly controlled by DOT1L. In contrast, most of the more highly-expressed genes downregulated in *Dot1L* KO were marked by H3K79me2 (Fig. 5a right panel and Sup Fig. 5b). This demonstrates that in normal CD8$^+$ T cells DOT1L-mediated H3K79 methylation generally marks expressed genes, but only a subset of the methylated genes needs H3K79 methylation for maintaining full expression levels. Thus, in normal T cells DOT1L does not act as a transcriptional switch but rather seems to be required for transcription maintenance of a subset of methylated genes that are already on and it indirectly promotes repression of genes.

Amongst the differentially expressed genes marked with H3K79me2, we searched for candidate direct target genes that could mediate the role of DOT1L in terminal T cell differentiation. We were especially interested in factors that could explain the prominent gene derepression in *Dot1L*-KO cells. To this end we selected genes that were significantly downregulated in KO and had harbored H3K79me2 at the 5' end of the gene, both in T_N and T_{CM}. We further narrowed the list down to genes that were annotated as "negative regulator of transcription by RNA polymerase II", resulting in 14 transcriptional regulators. Among those, *Ezh2* emerged as a potentially relevant target of DOT1L that could explain part of the derepression of genes in *Dot1L*-KO cells (Table 1). EZH2 is part of the Polycomb-repressive complex 2 (PRC2), which deposits H3K27me3 [54, 55, 56, 57, 58, 59], a mark involved in repression of developmentally-regulated genes and in switching off naïve and memory genes during terminal differentiation of effector $CD8^+$ T cells [40, 60]. Although the change in *Ezh2* mRNA expression was modest between WT and KO (Sup Fig. 5c), the *Ezh2* gene was H3K79me2 methylated (Sup Fig. 5d), and *Dot1L*-KO mice share several T-cell phenotypes with *Ezh2*-KO mice [40, 60], although this is dependent on the mouse model used [61, 62, 63]. To further investigate the idea that misregulation of PRC2 targets could be one of the downstream consequences of loss of DOT1L in $CD8^+$ T cells, we compared the gene expression changes in an *Ezh2*-KO model [61] with those seen in *Dot1L*-KO $CD8^+$ T cells. This revealed substantial overlap between the derepressed genes in the two models (Fig. 5b), suggesting a functional connection between two seemingly opposing epigenetic pathways. Furthermore, we determined H3K27me3 scores based on previous ChIP-Seq studies [64] and compared them with the gene expression in WT and *Dot1L*-KO SP $CD8^+$ thymocytes and peripheral $CD8^+$ T cells. This analysis showed that the genes that were upregulated in *Dot1L*-KO and lack H3K79me2 in WT were strongly enriched for H3K27me3 in WT memory precursor $CD8^+$ T cells (Fig. 5c). As a control, expression matched non-differentially expressed genes were not enriched for H3K27me3 (Fig. 5c). Taken together, these findings suggest that one of the consequences of loss of DOT1L-mediated H3K79me2 is derepression of a subset of PRC2 targets that are normally

actively repressed. This, together with the other transcriptional changes likely contributes to the perturbation of the epigenetic identity of $CD8^+$ T_{AIM} cells, thereby compromising their ability to terminally differentiate *in vivo*.

Discussion

The histone methyltransferase DOT1L has emerged as a druggable target in MLL-rearranged leukemia and additional roles in cancer have been suggested [22, 23, 24, 65, 66, 67, 68]. This in combination with the availability of highly-specific DOT1L inhibitors make DOT1L a potential target for cancer therapy. However, the role of DOT1L in normal lymphocyte physiology remained unknown. Here we show that DOT1L, plays a central role in ensuring normal T cell differentiation. To our knowledge, DOT1L is the first reported activating histone methyltransferase with a causal role in T cell differentiation.

T cell differentiation is intimately linked to epigenetic programming, but the mechanistic role of epigenetic marks in steering T cell differentiation [40, 60, 61, 63, 69, 70] and thymic selection [71, 72, 73, 74, 75] has only recently become more clear. Here we observed that ablation of *Dot1L* in the T cell lineage differentially affected $CD4^+$ and $CD8^+$ T cells. Following deletion of *Dot1L* by *Lck*-Cre during early thymocyte development, $CD4^+$ T cells were strongly reduced, while the number of $CD8^+$ T cells was increased. The fact that a substantial fraction of the remaining $CD4^+$ T cells had not lost DOT1L activity indicates that the $CD4^+$ compartment and especially regulatory T cells depend on DOT1L for their normal development. Further research exploring the dependency of $CD4^+$ T cells on DOT1L may provide novel strategies for immune modulation and treatment of $CD4^+$ T cell malignancies [76, 77].

In $CD8^+$ T cells, loss of DOT1L resulted in a massive gain of $CD44^+CD62L^+$ memory-like cells associated with a simultaneous loss of the naïve compartment. These cells start to acquire memory features intrathymically, express a diverse un-skewed TCRβ repertoire, and lack expression of CD49d. Taken together, this suggests that these memory-like $CD8^+$ T cells arose independently of foreign antigens, leading us to designate these cells as antigen-independent memory-like T_{AIM} $CD8^+$ cells. Importantly,

such unconventional memory-phenotype cells constitute a substantial (15-25%) fraction of the peripheral $CD8^+$ T cell compartment in WT mice and humans [4, 35, 44, 78, 79]. The fraction of unconventional memory-phenotype T cells further increases with age [80, 81]. The biological role of antigen-inexperienced memory $CD8^+$ T cells is still not completely understood, but these cells have been observed to respond more rapidly to TCR activation than T_N cells and they have been suggested to provide by-stander protection against infection in an antigen-independent way [34, 44]. However, in older mice, virtual memory cells have been reported to lose their proliferative potential and acquire characteristics of senescence [82]. The mechanism of unconventional memory-phenotype differentiation is also poorly understood [2]. In some mouse models $CD8^+$ T cells differentiate upon excess production of IL-4 by iNKT or γδ T cells [3, 39, 83, 84, 85, 86]. In contrast, other mouse models report that antigen inexperienced memory $CD8^+$ T cell differentiation is cell intrinsic [87, 88]. Here we show that DOT1L plays an important role in T_{AIM} $CD8^+$ cell differentiation by cell-intrinsic mechanisms.

It has been established in several independent mouse models that the quality of TCR signaling closely relates to the formation of T_{AIM} cells [34, 43, 44]. Our results show that loss of DOT1L leads to reduced surface expression of the CD3/TCR complex and co-receptors. This phenotype is likely related to the reduced expression of CD3ζ (Cd247), a target of DOT1L and a rate limiting molecule for assembly and transport of TCR/CD3 complexes to the cell surface [1, 45, 46, 47, 48]. The failure to upregulate the TCR/CD3 complex upon positive selection likely prohibits differentiation of conventional T_N and supports formation of T_{AIM} cells. In addition, *Dot1L* ablation perturbed expression of TCR signaling genes, including *Itk* (IL2-inducible T cell kinase; a member of the Tec kinase family). Disruption of ITK signaling has also been reported to lead to antigen-independent T-cell differentiation [49]. Together, this suggests that one of the key functions of DOT1L is to ensure adequate TCR surface expression and signaling to maintain naivety and prevent T_{AIM} cell differentiation. The discovery of DOT1L as a key player in preventing

premature antigen-independent differentiation towards memory-type cells warrants further investigation and will aid in further uncovering the origin and regulation of this emerging and intriguing subset of the immune system.

Functionally, *Dot1L*-KO CD8$^+$ T_{AIM} cells partially displayed features of memory cells *in vitro* but *in vivo* showed an impaired immune response against *Listeria monocytogenes*. The rapid differentiation towards effector cells suggests that *Dot1L*-KO T_{AIM} cells might execute a partial by-stander response, but DOT1L appears to be required to accomplish full effector function. Interestingly, similar features have been observed for virtual memory cells [44]. The reduced TCR density and affected TCR signaling network in *Dot1L*-KO T cells likely further contribute to the impaired immune response.

How does DOT1L affect T cell differentiation at the chromatin level? Inspection of the transcriptome and epigenome provided evidence that DOT1L methylates transcriptionally active genes in T cells and positively affects gene expression. However, only a subset of the targets required DOT1L for maintenance of normal expression levels, which is in agreement with previous observations [89, 90]. Why some genes depend on DOT1L/H3K79 methylation and others not is not known yet although a recent study indicates that in MLL-rearranged leukemic cell lines some genes harbor a 3' enhancer located in the H3K79me2/3 marked genic region, which can make them more sensitive to loss of DOT1L [89].

One of the genes that was H3K79 methylated and dependent on DOT1L in normal peripheral CD8$^+$ T cells was *Ezh2*. Of note, *Ezh2* expression was not reduced in *Dot1L* KO CD8 SP thymocytes. Importantly, analysis of data from [26] et al. showed that *Ezh2* expression is also reduced in human T cells in which DOT1L was inactivated not by deletion but by treatment with a DOT1L inhibitor (Sup Fig. 5e). This suggests that the epigenetic crosstalk that we uncovered in mice is evolutionarily conserved. However,

the exact mechanisms by which DOT1L affects EZH2/PRC2 activity are still unknown. Although PRC2 targets were derepressed, *Ezh2* mRNA expression was only modestly reduced in *Dot1L*-KO peripheral T cells, suggesting that DOT1L not only affects expression of *Ezh2* but might also be involved in other processes that regulate PRC2 activity, such as the stability, structure, recruitment, or localization of the PRC2 complex [59, 62, 91, 92, 93, 94, 95, 96, 97, 98, 99, 100]. H3K79 methylation is not likely to promote H3K27 methylation directly at the level of nucleosomes because the modifications generally occur in different genic regions and mark different sets of genes (e.g. see Fig. 5C) Interestingly, recruitment of DOT1L to nucleosomes by its interaction partner AF10 has been shown to be negatively affected by methylation of H3K27 [101]. Therefore, the crosstalk between DOT1L and PRC2 might involve mutual interactions. Restricting DOT1L to nucleosomes unmethylated at H3K27 might be one of the mechanisms by which H3K79me and H3K27me3 are directed to non-overlapping sites, as we also observed in T cells (Fig. 5C).

Derepression of some of the targets of PRC2 is just one of the consequences of loss of DOT1L. Besides *Ezh2*, DOT1L affects the expression of other genes, including several additional candidate transcription regulators (Table 1). In the future, it will be important to determine other mechanisms by which DOT1L affects the $CD8^+$ T cell transcriptome to fully understand its central role in $CD8^+$ T cell biology. Finally, we cannot exclude that DOT1L has additional methylation targets besides H3K79 that contribute to role of DOT1L in safeguarding T cell differentiation and effector functions. Although understanding the mechanisms in more detail will require further studies, the role of DOT1L in preventing premature differentiation and safeguarding the epigenetic identity is conserved in other lymphocyte subsets. In an accompanying study (Aslam et al) , we observed in an independent mouse model that loss of *Dot1L* in B cells also led to premature differentiation, perturbed repression of PRC2 targets, and a compromised humoral immune response. Therefore, DOT1L is emerging as a central epigenetic regulator of lymphocyte differentiation and functionality.

In conclusion, we identify H3K79 methylation by DOT1L as an activating epigenetic mark critical for $CD8^+$ T cell differentiation and maintenance of epigenetic identity. Further investigation into the central role of the druggable epigenetic writer DOT1L in lymphocytes is likely to provide novel strategies for immune modulations and disease intervention [102, 103, 104, 105].

Methods

Mice

Lck-Cre*;Dot1L*$^{fl/fl}$ mice have been described elsewhere previously [25] and were based on the Dot1Ltm1a(KOMP)Wtsi line generated by the Wellcome Trust Sanger Institute (WTSI) and obtained from the KOMP Repository (www.komp.org) [106]. Mice from this newly created *Lck*-Cre*;Dot1L* strain were breeding in a mendelian ratio and had no welfare issues. *Lck*-Cre$^{+/-}$*;Dot1L*$^{fl/fl}$ (KO) mice were compared to *Lck*-Cre$^{+/-}$*;Dot1L*$^{wt/wt}$ (WT) mice and were indicated with *Lck*-Cre$^{+/-}$*;Dot1L*$^{fl/wt}$ (Het) mice in order to eliminate any Cre-specific effects [107]. The *Lck*-Cre*;Dot1L*$^{fl/fl}$ mice were crossed with OT(B6J) mice (a kind gift from the Ton Schumacher group, originally from Jackson labs) to generate *Lck*-Cre*;Dot1L*$^{fl/fl}$*;OT-I* mice. Both strains were bred in-house. Mice used for experiments were between 6 weeks and 8 months old and of both genders. For each individual experiment mice were matched for age and gender. Mice were housed under specific pathogen free (SPF) conditions at the animal laboratory facility of the Netherlands Cancer Institute (NKI; Amsterdam, Netherlands). All experiments were approved by the Animal Ethics Committee of the NKI and performed in accordance with institutional, national and European guidelines for animal care and use.

Flow cytometry

Single cell suspensions were made from spleen and thymus. Erylysis was performed on blood and spleen samples. Cells were stained with fluorescently labeled antibodies in a 1:200 dilution unless otherwise indicated (Table 2). Of note, for OT-I tetramer stains the CD8 antibody clone 53-6.7 was used [108]. For intracellular staining, cells were fixed and permeabilized using the Transcription Factor Buffer kit (Benton Dickinson). Antibodies for intracellular staining were diluted 1:200 in Perm/Wash buffer (Table 3). For H3K79me2 staining, cells were first stained with surface markers and fixed and permeabilized as

described before. After fixation and permeabilization cells were washed with Perm/Wash containing 0.25% SDS. α-H3K79me2 (Millipore) was diluted 1:200 into Perm/Wash + 0.25% SDS and cells were incubated for 30 min. Cells were washed with Perm/Wash and incubated with the secondary antibodies Donkey anti-Rabbit AF555 (Thermo Scientific) or Goat-anti-Rabbit AF488 (Invitrogen) 1:1000 in Perm/Wash. Flow cytometry was performed using the LSR Fortessa (BD Biosciences) and data were analyzed with FlowJo software (Tree Star inc.) Histograms were smoothed.

Immunohistochemistry

Thymus tissues were fixed in EAF (ethanol, acetic acid, formol saline) for 24 hours and subsequently embedded in paraffin. Immunohistochemistry was performed with H3K79me2 antibody [109]as described in [25].

PCR

Sorted $CD4^+$ and $CD8^+$ T cells were lysed in DirectPCR Lysis Reagent (mouse tail) (Viagen Biotech) with 1mg/ml proteinase K (Sigma). *Dot1L*$^{fl/fl}$ and *Dot1L*$^{\Delta/\Delta}$ was detected by PCR using the following primers. Dot1L_FWD: GCAAGCCTACAGCCTTCATC, Dot1L_REV: CACCGGATAGTCTCAATAATCTCA and Dot1L_Δ: GAACCACAGGATGCTTCAG and MyTaq Red Mix (GC Biotech).

In vitro stimulation

To determine cytokine production upon *in vitro* stimulation, splenocytes were stimulated with 20 ng/ml PMA (Sigma), 0.5 µg/ml Ionomcyin (Sigma) and 1µl/ml Golgi Plug protein transport inhibitor (Benton Dickinson) for 4 hours. Cells were stained as described above. To determine proliferation and IFNγ production upon *in vitro* TCR-mediated stimulation splenocytes were enriched for T cells using CD19 microbeads depletion (Miltenyi Biotec) on LS columns (Miltenyi Biotec). Cells were labeled with 0.5mM

CFSE (Thermo Scientific) in order to measure proliferation and left unlabeled to determine IFNγ production and plated in a 96-wells plate coated with anti-CD3 (145-2C11) (BD) in complete medium (IMDM supplemented with 8% FCS, 100 mM pen/strep and 100 mM β-mercaptoethanol). Anti-CD28 (37.51) (BD) was added to the medium and cells were incubated at 37 ^{o}C with 5% CO_2. At day 1 after CFSE labeling, cells were analyzed by flow cytometry to confirm the uptake of CFSE. In order to determine IFNγ production cells were incubated with Golgi Plug protein transport inhibitor (Benton Dickinson) for 4 hours.

In vivo immunization with *Listeria monocytogenes*

Listeria monocytogenes strain LM-OVA was a gift from Ton Schumacher (NKI). Bacteria were grown overnight in Bacto Brain Heart Infusion, Porcine (BHI) medium (BD) to an absorbance at 600 nm of OD 0.9. A sub-lethal dose (10.000 colony forming units; CFUs) of *Listeria monocytogenes* in HBSS was injected intravenously into the mice. The number of bacteria injected was confirmed by growth on BHI agar plates (BD) with 25 µg/ml chloramphenicol. The immune response was followed in the blood by taking blood samples via tail vein puncture at day -3 and +4. The CFUs were determined for spleen and liver. Single-cell suspensions were made in PBS and the cells were lysed in 0.1 % IGEPAL. Homogenized suspensions were plated on BHI agar plates in three dilutions (undiluted, 1:10 and 1:100). After 48 hours colony counts were determined.

Sort for RNA-Seq, ChIP-Seq and TCR-Seq

For cell sorting, thymus and spleen samples were homogenized. Erylysis was performed on spleen samples. Cells were stained with fluorescently labeled antibodies (1:200) (Table 4) and sorted on FACSAria Ilu (BD Biosciences), FACSAria Fusion (BD Biosciences) or MoFlo Astrios (Beckman Coulter). Cells were collected in tubes coated with FCS.

RNA-Seq sample preparation

Flow cytometrically purified cells were resuspended in Trizol (Ambion Life Technologies) and total RNA was extracted according to the manufacturer's protocol. Quality and quantity of the total RNA was assessed by the 2100 Bioanalyzer using a Nano chip (Agilent). Only RNA samples having an RNA Integrity Number (RIN) > 8 were subjected to library generation.

RNA-Seq library preparation

Strand-specific cDNA libraries were generated using the TruSeq Stranded mRNA sample preparation kit (Illumina) according to the manufacturer's protocol. The libraries were analyzed for size and quantity of cDNAs on a 2100 Bioanalyzer using a DNA 7500 chip (Agilent), diluted and pooled in multiplex sequencing pools. The libraries were sequenced as 65 base single reads on a HiSeq2500 (Illumina).

RNA-Seq data preprocessing

RNA-Seq reads were mapped to mm10 (Ensembl GRCm38) using TopHat with the arguments `--prefilter-multihits –no-coverage-search –bowtie1 –library-type fr-firststrand` using a transcriptome index. Counts per gene were obtained using htseq-count with the options `-m union -s no` and Ensembl GRCm38.90 gene models. Analysis was restricted to genes that have least 20 counts in at least 4 samples, and at least 5 counts in 4 samples in specific contrasts, to exclude very low abundance genes. Differential expression analysis was performed on only relevant samples using DESeq2 and default arguments with the design set to either *Dot1L*KO status or cell type. Adaptive effect size shrinkage was performed with the ashr R package to control for the lower information content in low abundance transcripts. Genes were considered to be differentially expressed when the p-value of the negative binomial Wald test was below 0.01 after the Benjamini-Hochberg multiple testing correction. Sets of differentially expressed

genes in indicated conditions were called 'gene signatures'. An exception was made for the Ezh2 RNA-Seq data from He et al., [61] wherein the dispersion was estimated with a local fit, using `estimateDispersion` function in DESeq2 with the argument `fitType = "local"` and using an adjusted p-value cutoff of 0.05, to increase the number of detected differential genes. Principal component analysis was performed using the `prcomp` function on variance stabilizing transformed data of all samples with the `vst` function from the DESeq2 package on all samples using default arguments. For analyses where we performed expression matching, we chose genes with an absolute log2 fold changes less than 0.1 and false discovery rate corrected p-values above 0.05 that were closest in mean expression to each of the genes being matched without replacement.

ChIP-Seq sample preparation

Sorted cells were centrifuged at 500 rcf. The pellet was resuspended in IMDM containing 2% FCS and formaldehyde (Sigma) was added to a final concentration of 1%. After 10 min incubation at RT glycine (final concentration 125 mM) was added and incubated for 5 min. Cells were washed twice with ice-cold PBS containing Complete, EDTA free, protein inhibitor cocktail (PIC) (Roche). Cross-linked cell pellets were stored at -80 ^{o}C. Pellets were resuspended in cold Nuclei lysis buffer (50mM Tris-HCl pH 8.0, 10mM EDTA pH8.0, 1%SDS) + PIC and incubated for at least 10 min. Cells were sonicated with PICO to an average length of 200-500bp using 30s on/ 30s off for 3 min. After centrifugation at high speed debris was removed and 9x volume of ChIP dilution buffer (50mM Tris-HCl pH8, 0.167M NaCl, 1.1% Triton X-100, 0.11% sodium deoxycholate) + PIC and 5x volume of RIPA-150(50mM Tris-HCl pH8, 0.15M NaCl, 1mM EDTA pH8, 0.1% SDS, 1% Triton X-100, 0.1% sodium deoxycholate) + PIC was added. Shearing efficiency was confirmed by reverse crosslinking the chromatin and checking the size on agarose gel. Chromatin was pre-cleared by adding ProteinG Dynabeads (Life Technologies) and rotation for 1 hour at 4 ^{o}C. After the beads were removed 2µl H3K79me1, 2µl H3K79me2 (NL59, Merck Millipore) and 1µl

H3K4me3 (ab8580, Abcam) were added and incubated overnight at 4°C. ProteinG Dynabeads were added to the IP and incubated for 3 hours at 4 ^{o}C. Beads with bound immune complexes were subsequently washed with RIPA-150, 2 times RIPA-500 (50mM Tris-HCl pH8, 0.5M NaCl, 1mM EDTA pH8, 0.1% SDS, 1% Triton X-100, 0.1% sodium deoxycholate), 2 times RIPA-LiCl (50mM Tris-HCl pH8, 1mM EDTA pH8, 1% Nonidet P-40, 0.7% sodium deoxycholate, 0.5M LiCl2) and TE. Beads were resuspended in 150 µl Direct elution buffer (10mM Tris-HCl pH8, 0.3M NaCl, 5mM EDTA pH8, 0.5%SDS) and incubated overnight at 65 ^{o}C and input samples were included. Supernatant was transferred to a new tub and 1µl RNAse A (Sigma) and 3 µl ProtK (Sigma) was added per sample and incubated at 55 ^{o}C for 1 hour. DNA was purified using Qiagen purification columns.

ChIP-Seq Library preparation

Library preparation was done using KAPA LTP Library preparation kit using the manufacturer's protocol with slight modifications. Briefly, after end-repair and A-tailing adaptor were ligated followed by Solid Phase Reverisble Immobilization (SPRI) clean-up. Libraries were amplified by PCR and fragments between 250-450 bp were selected using AMPure XP beads (Beckman Coultier). The libraries were analyzed for size and quantity of DNAs on a 2100 Bioanalyzer using a High Sensitivity DNA Kit (Agilent), diluted and pooled in multiplex sequencing pools. The libraries were sequenced as 65 base single reads on a HiSeq2500 (Illumina).

ChIP-Seq data preprocessing

ChIP-Seq samples were mapped to mm10 (Ensembl GRCm38) using BWA-MEM with the option '-M' and filtered for reads with a mapping quality higher than 37. Duplicate reads were removed using MarkDuplicates from the Picard toolset with `VALIDATION_STRINGENCY=LENIENT` and `REMOVE_DUPLICATES=false` as argument. Low quality reads with any FLAG bit set to 1804 were

removed. Bigwig tracks were generated by using bamCoverage from deepTools using the following arguments: `-of bigwig –binsize 25 –normalizeUsing RPGC –ignoreForNormalization chrM –effectiveGenomeSize 2652783500`. For visualization of heatmaps and genomic tracks, bigwig files were loaded into R using the `import.bw()` function from the rtracklayer R package. TSSs for heatmaps were taken from Ensembl GRCm38.90 gene models by taking the first base pair of the 5' UTR of transcripts. When such annotation was missing, the most 5' position of the first exon was taken.

Defining DOT1L targets involved in transcription regulation

Genes were selected that are down in KO with adjusted p-value < 0.01, with H3K79me2 normalized reads > 20 and the GO annotation "negative regulator of transcription by RNA polymerase II".

TCRβ-Seq

Between 100,000 and 1,100,000 sorted cells were used for TCRβ-Seq. DNA was extracted using Qiagen DNA isolation kit (Qiagen) and collected in 50 µl TE buffer. The concentration was determined with Nanodrop. Samples were sequenced and processed by Adaptive Biotechnologies using immunoSEQ mm TCRB Service (Survey).

Statistics

Statistical analyses were performed using Prism 7 (Graphpad). Data are presented as means ±SD unless otherwise indicated in the figure legends. The unpaired Student's t-test with two-tailed distributions was used for statistical analyses. A p-value <0.05 was considered statistically significant. * $p < 0.05$, ** $p < 0.01$, *** $p < 0.001$.

Acknowledgements

We thank the NKI animal pathology facility for histology and immunohistochemistry, as well as advice, the NKI genomics core facility for library preparations and sequencing, the NKI Flow Cytometry facility for assistance, the NKI Animal Laboratory Intervention Unit for performing immunization experiments, and the caretakers of the NKI Animal Laboratory facility for assistance and excellent animal care. The following reagent(s) was/were obtained through the NIH Tetramer Core Facility: CD1d-PBS57 and CD1d-unloaded tetramer. We thank Paul van den Berk for advice and Cheyenne Seerden for help with the flow cytometry experiments, Ton Schumacher and group for OT-I mice and OT-I tetramer, and Jan-Hermen Dannenberg for providing the Lck-Cre mouse model. We thank Muddassir Malik for critically reading the manuscript.

This work was supported by the Dutch Cancer Society (NKI2014-7232 to FvL and HJ) and the Netherlands Organisation for Scientific Research (NWO-VICI-016.130.627 to FvL; ZonMW Top 91213018 to HJ; ZonMW Top91218022 to FvL and HJ). The funders had no role in study design, data collection and interpretation, or the decision to submit the work for publication.

Author contributions

EMK-M, MAA, MFA, FvL and HJ jointly designed the experiments

EMK-M, MAA, MFA jointly carried out the experiments

CMM, HV, CL, and SH generated the mouse model and performed the initial analyses on thymocytes

TvW performed genotyping and ChIP experiments

TvdB, MAA, TK, MFA, and EdW performed bioinformatics analyses

DvD and JMMdH performed the initial characterization of splenocytes

TA and JB contributed to the immunization experiments

FvL and HJ designed and supervised the studies.

EMK-M, MAA, MFA, FvL and HJ wrote the manuscript

References

1. Borst, J., Jacobs, H. & Brouns, G. Composition and function of T-cell receptor and B-cell receptor complexes on precursor lymphocytes. *Curr. Opin. Immunol.* **8**, 181-190 (1996).
2. Hussain, T. & Quinn, K.M. Similar but different: Virtual memory CD8 T cells as a memory-like cell population. *Immunol. Cell Biol.* **97**, 675-684 (2019).
3. Jameson, S.C., Lee, Y.J. & Hogquist, K.A. Innate memory T cells. *Adv. Immunol.* **126**, 173-213 (2015).
4. White, J.T., Cross, E.W. & Kedl, R.M. Antigen-inexperienced memory CD8(+) T cells: where they come from and why we need them. *Nat. Rev. Immunol.* **17**, 391-400 (2017).
5. Henning, A.N., Roychoudhuri, R. & Restifo, N.P. Epigenetic control of CD8(+) T cell differentiation. *Nat. Rev. Immunol.* **18**, 340-356 (2018).
6. Gray, S.M., Kaech, S.M. & Staron, M.M. The interface between transcriptional and epigenetic control of effector and memory CD8 + T-cell differentiation. *Immunol. Rev.* **261**, 157-168 (2014).
7. Omilusik, K.D. & Goldrath, A.W. Remembering to remember: T cell memory maintenance and plasticity. *Curr. Opin. Immunol.* **58**, 89-97 (2019).
8. Abdelsamed, H.A., Zebley, C.C. & Youngblood, B. Epigenetic Maintenance of Acquired Gene Expression Programs during Memory CD8 T Cell Homeostasis. *Front. Immunol.* **9**, 6-6 (2018).
9. Weng, N.-p., Araki, Y. & Subedi, K. The molecular basis of the memory T cell response: differential gene expression and its epigenetic regulation. *Nat. Rev. Immunol.* **12**, 306-315 (2012).
10. Phan, A.T., Goldrath, A.W. & Glass, C.K. Metabolic and Epigenetic Coordination of T Cell and Macrophage Immunity. *Immunity* **46**, 714-729 (2017).
11. Vlaming, H. & van Leeuwen, F. The upstreams and downstreams of H3K79 methylation by DOT1L. *Chromosoma* **125**, 593-605 (2016).
12. Steger, D.J. *et al.* DOT1L/KMT4 recruitment and H3K79 methylation are ubiquitously coupled with gene transcription in mammalian cells. *Mol. Cell. Biol.* **28**, 2825-2839 (2008).
13. Xiao, Z., Chen, L., Zhou, Q. & Zhang, W. Dot1l deficiency leads to increased intercalated cells and upregulation of V-ATPase B1 in mice. *Exp. Cell Res.* **344**, 167-175 (2016).
14. Cecere, G., Hoersch, S., Jensen, M.B., Dixit, S. & Grishok, A. The ZFP-1(AF10)/DOT-1 complex opposes H2B ubiquitination to reduce Pol II transcription. *Molecular Cell* **50**, 894-907 (2013).
15. Chory, E.J. *et al.* Nucleosome Turnover Regulates Histone Methylation Patterns over the Genome. *Mol. Cell* **73**, 1-12 (2018).
16. Schubeler, D. *et al.* The histone modification pattern of active genes revealed through genome-wide chromatin analysis of a higher eukaryote. *Genes Dev.* **18**, 1263-1271 (2004).
17. Wood, K., Tellier, M. & Murphy, S. DOT1L and H3K79 Methylation in Transcription and Genomic Stability. *Biomolecules* **8** (2018).
18. Zhang, W., Xia, X., Reisenauer, M.R., Hemenway, C.S. & Kone, B.C. Dot1a-AF9 complex mediates histone H3 Lys-79 hypermethylation and repression of ENaCalpha in an aldosterone-sensitive manner. *J. Biol. Chem.* **281**, 18059-18068 (2006).
19. McLean, C.M., Karemaker, I.D. & van Leeuwen, F. The emerging roles of DOT1L in leukemia and normal development. *Leukemia* **28**, 2131-2138 (2014).
20. Zhang, Y. & Kutateladze, T.G. Methylation of Histone H3K79 by Dot1L Requires Multiple Contacts with the Ubiquitinated Nucleosome. *Mol. Cell* **74**, 862-863 (2019).
21. Onder, T.T. *et al.* Chromatin-modifying enzymes as modulators of reprogramming. *Nature* **483**, 598-602 (2012).
22. Bernt, K.M. *et al.* MLL-rearranged leukemia is dependent on aberrant H3K79 methylation by DOT1L. *Cancer cell* **20**, 66-78 (2011).
23. Stein, E.M. *et al.* The DOT1L inhibitor pinometostat reduces H3K79 methylation and has modest clinical activity in adult acute leukemia. *Blood* **131**, 2661-2669 (2018).
24. Okada, Y. *et al.* Leukaemic transformation by CALM–AF10 involves upregulation of Hoxa5 by hDOT1L. *Nat. Cell Biol.* **8**, 1017-1024 (2006).
25. Vlaming, H. *et al.* Conserved crosstalk between histone deacetylation and H3K79 methylation generates DOT1L-dose dependency in HDAC1-deficient thymic lymphoma. *EMBO J.* **38**, e101564-e101564 (2019).
26. Kagoya, Y. *et al.* DOT1L inhibition attenuates graft-versus-host disease by allogeneic T cells in adoptive immunotherapy models. *Nat. Comm.* **9** (2018).
27. Scheer, S. *et al.* A chemical biology toolbox to study protein methyltransferases and epigenetic signaling. *Nat. Comm.* **10** (2019).
28. Jones, B. *et al.* The histone H3K79 methyltransferase Dot1L is essential for mammalian development and heterochromatin structure. *PloS Genetics* **4**, e1000190-e1000190 (2008).
29. Feng, Y. *et al.* Early mammalian erythropoiesis requires the Dot1L methyltransferase. *Blood* **116**, 4483-4491 (2010).

30. De Vos, D. *et al.* Progressive methylation of ageing histones by Dot1 functions as a timer. *EMBO Rep.* **12**, 956-962 (2011).
31. Vlaming, H. *et al.* Direct screening for chromatin status on DNA barcodes in yeast delineates the regulome of H3K79 methylation by Dot1. *Elife* **5** (2016).
32. Radman-Livaja, M. *et al.* Patterns and mechanisms of ancestral histone protein inheritance in budding yeast. *PLoS Biol.* **9**, e1001075 (2011).
33. Truckenbrod, E.N. & Jameson, S.C. The virtuous self-tolerance of virtual memory T cells. *EMBO J.* **37**, e99883-e99883 (2018).
34. Drobek, A. *et al.* Strong homeostatic TCR signals induce formation of self-tolerant virtual memory CD8 T cells. *EMBO J.* **37**, e98518-e98518 (2018).
35. Haluszczak, C. *et al.* The antigen-specific CD8 + T cell repertoire in unimmunized mice includes memory phenotype cells bearing markers of homeostatic expansion. *J. Exp. Med.* **206**, 435-448 (2009).
36. Martinet, V. *et al.* Type i interferons regulate eomesodermin expression and the development of unconventional memory CD8(+) T cells. *Nat. Comm.* **6**, 7089-7089 (2015).
37. Intlekofer, A.M. *et al.* Effector and memory CD8+ T cell fate coupled by T-bet and eomesodermin. *Nat. Immunol.* **6**, 1236-1244 (2005).
38. Lee, J.-Y.Y., Hamilton, S.E., Akue, A.D., Hogquist, K.A. & Jameson, S.C. Virtual memory CD8T cells display unique functional properties. *Proc. Natl. Acad. Sci. U.S.A.* **110**, 13498-13503 (2013).
39. Atherly, L.O. *et al.* The Tec Family Tyrosine Kinases Itk and Rlk Regulate the Development of Conventional CD8+ T Cells. *Immunity* **25**, 79-91 (2006).
40. Kakaradov, B. *et al.* Early transcriptional and epigenetic regulation of CD8 + T cell differentiation revealed by single-cell RNA sequencing. *Nat. Immunol.* **18**, 422-432 (2017).
41. Wingender, G. *et al.* Immediate antigen-specific effector functions by TCR-transgenic CD8+ NKT cells. *Eur. J. Immunol.* **36**, 570-582 (2006).
42. Fenton, R.G., Marrack, P., Kappler, J.W., Kanagawa, O. & Seidman, J.G. Isotypic exclusion of γδ T cell receptors in transgenic mice bearing a rearranged β-chain gene. *Science* **241**, 1089-1092 (1988).
43. Renkema, K.R., Li, G., Wu, A., Smithey, M.J. & Nikolich-Žugich, J. Two separate defects affecting true naive or virtual memory T cell precursors combine to reduce naive T cell responses with aging. *J. Immunol.* **192**, 151-159 (2014).
44. White, J.T. *et al.* Virtual memory T cells develop and mediate bystander protective immunity in an IL-15-dependent manner. *Nat. Comm.* **7**, 11291-11291 (2016).
45. DeFord-Watts, L.M. *et al.* The CD3 ζ Subunit Contains a Phosphoinositide-Binding Motif That Is Required for the Stable Accumulation of TCR–CD3 Complex at the Immunological Synapse. *J. Immunol.* **186**, 6839-6847 (2011).
46. Call, M.E. & Wucherpfennig, K.W. The T Cell Receptor: Critical Role of the Membrane Environment in Receptor Assembly and Function. *Annu. Rev. Immunol.* **23**, 101-125 (2005).
47. Baniyash, M. TCR ζ-chain downregulation: Curtailing an excessive inflammatory immune response. *Nat. Rev. Immunol.* **4**, 675-687 (2004).
48. Ashwell, J.D. & Klausner, R.D. Genetic and Mutational Analysis of the T-Cell Antigen Receptor. *Annu. Rev. Immunol.* **8**, 139-167 (1990).
49. Nayar, R. *et al.* TCR signaling via Tec kinase ITK and interferon regulatory factor 4 (IRF4) regulates CD8+ T-cell differentiation. *Proc. Natl. Acad. Sci. U.S.A.* **109**, E2794-E2802 (2012).
50. Hogquist, K.A. *et al.* T cell receptor antagonist peptides induce positive selection. *Cell* **76**, 17-27 (1994).
51. Kaech, S.M., Wherry, E.J. & Ahmed, R. Effector and memory T-cell differentiation: implications for vaccine development. *Nat. Rev. Immunol.* **2**, 251-262 (2002).
52. Mannering, S.I., Zhong, J. & Cheers, C. T-cell activation, proliferation and apoptosis in primary Listeria monocytogenes infection. *Immunology* **106**, 87-95 (2002).
53. Huff, J.T., Plocik, A.M., Guthrie, C. & Yamamoto, K.R. Reciprocal intronic and exonic histone modification regions in humans. *Nat. Struct. Mol. Biol.* **17**, 1495-1499 (2010).
54. Margueron, R. & Reinberg, D. The Polycomb complex PRC2 and its mark in life. *Nature* **469**, 343-349 (2011).
55. Yu, J.-R., Lee, C.-H., Oksuz, O., Stafford, J.M. & Reinberg, D. PRC2 is high maintenance. *Genes Dev.* **33**, 903-935 (2019).
56. van Mierlo, G., Veenstra, G.J.C., Vermeulen, M. & Marks, H. The Complexity of PRC2 Subcomplexes. *Trends Cell Biol.* **29**, 660-671 (2019).
57. Holoch, D. & Margueron, R. Mechanisms Regulating PRC2 Recruitment and Enzymatic Activity. *Trends. Biochem. Sci.* **42**, 531-542 (2017).
58. Healy, E. *et al.* PRC2.1 and PRC2.2 Synergize to Coordinate H3K27 Trimethylation. *Mol. Cell* (2019).
59. Moritz, L.E. & Trievel, R.C. Structure, mechanism, and regulation of polycomb-repressive complex 2. *J. Biol. Chem.* **293**, 13805-13814 (2018).

60. Gray, S.M., Amezquita, R.A., Guan, T., Kleinstein, S.H. & Kaech, S.M. Polycomb Repressive Complex 2-Mediated Chromatin Repression Guides Effector CD8+ T Cell Terminal Differentiation and Loss of Multipotency. *Immunity* **46**, 596-608 (2017).
61. He, S. *et al.* Ezh2 phosphorylation state determines its capacity to maintain CD8+ T memory precursors for antitumor immunity. *Nat. Comm.* **8** (2017).
62. Ji, Y. *et al.* miR-155 harnesses Phf19 to potentiate cancer immunotherapy through epigenetic reprogramming of CD8 + T cell fate. *Nat. Comm.* (2019).
63. Chen, G. *et al.* Ezh2 Regulates Activation-Induced CD8+ T Cell Cycle Progression via Repressing Cdkn2a and Cdkn1c Expression. *Front. Immunol.* **9** (2018).
64. Yu, B. *et al.* Epigenetic landscapes reveal transcription factors that regulate CD8+T cell differentiation. *Nat. Immunol.* **18**, 573-582 (2017).
65. Zhu, B. *et al.* The protective role of DOT1L in UV-induced melanomagenesis. *Nat. Comm.* **9**, 259-259 (2018).
66. Salgado, C. *et al.* A novel germline variant in the DOT1L gene co-segregating in a Dutch family with a history of melanoma. *Melanoma Res.* **[Epub ahead of print]** (2019).
67. Zhang, X. *et al.* Prognostic and therapeutic value of disruptor of telomeric silencing-1-like (DOT1L) expression in patients with ovarian cancer. *J. Hematol. Oncol.* **10**, 1-13 (2017).
68. Wong, M. *et al.* The Histone Methyltransferase DOT1L Promotes Neuroblastoma by Regulating Gene Transcription. *Cancer Res.* **77** (2017).
69. Pace, L. *et al.* The epigenetic control of stemness in CD8+ T cell fate commitment. *Science* **359**, 177-186 (2018).
70. Newman, D.M. *et al.* Acetylation of the Cd8 Locus by KAT6A Determines Memory T Cell Diversity. *Cell Rep.* **16**, 3311-3321 (2016).
71. Kasler, H.G. *et al.* Histone Deacetylase 7 Regulates Cell Survival and TCR Signaling in CD4/CD8 Double-Positive Thymocytes. *J. Immunol.* **186**, 4782-4793 (2011).
72. Kasler, H.G. & Verdin, E. Histone Deacetylase 7 Functions as a Key Regulator of Genes Involved in both Positive and Negative Selection of Thymocytes. *Mol. Cell. Biol.* **27**, 5184-5200 (2007).
73. Dequiedt, F. *et al.* HDAC7, a thymus-specific class II histone deacetylase, regulates Nur77 transcription and TCR-mediated apoptosis. *Immunity* **18**, 687-698 (2003).
74. Stengel, K.R., Zhao, Y., Klus, N.J., Kaiser, J.F. & Gordy, L.E. Histone Deacetylase 3 is Required for Efficient T-cell Development. *Mol. Cell. Biol.* **35**, 3854-3865 (2015).
75. Philips, R.L. *et al.* HDAC3 restrains CD8-lineage genes to maintain a bi-potential state in CD4+CD8+ thymocytes for CD4-lineage commitment. *eLife* **8** (2019).
76. Salah, E. Primary cutaneous CD4+ small/medium pleomorphic T-cell lymphoproliferative disorder: Where do we stand? A systematic review. *JDDG* **17**, 123-136 (2019).
77. Pulitzer, M. Cutaneous T-cell Lymphoma. *Clin. Lab. Med.* **37**, 527-546 (2017).
78. Akue, A.D., Lee, J.-Y. & Jameson, S.C. Derivation and Maintenance of Virtual Memory CD8 T Cells. *J. Immunol.* **188**, 2516-2523 (2012).
79. Barbarin, A. *et al.* Phenotype of NK-like CD8(+) T cells with innate features in humans and their relevance in cancer diseases. *Front. Immunol.* **8**, 316-316 (2017).
80. Chiu, B.-C.C., Martin, B.E., Stolberg, V.R. & Chensue, S.W. Cutting edge: Central memory CD8 T cells in aged mice are virtual memory cells. *J. Immunol.* **191**, 5793-5796 (2013).
81. Lanzer, K.G., Cookenham, T., Reiley, W.W. & Blackman, M.A. Virtual memory cells make a major contribution to the response of aged influenza-naïve mice to influenza virus infection. *Immun. Ageing* **15**, 1-13 (2018).
82. Quinn, K.M. *et al.* Age-Related Decline in Primary CD8+ T Cell Responses Is Associated with the Development of Senescence in Virtual Memory CD8+ T Cells. *Cell Rep.* **23**, 3512-3524 (2018).
83. Felices, M., Yin, C.C., Kosaka, Y., Kang, J. & Berg, L.J. Tec kinase Itk in γδT cells is pivotal for controlling IgE production in vivo. *Proc. Natl. Acad. Sci. U.S.A.* **106**, 8308-8308 (2009).
84. Vasanthakumar, A. *et al.* A non-canonical function of Ezh2 preserves immune homeostasis. *EMBO Rep.* **18**, 619-631 (2017).
85. Dobenecker, M.-W. *et al.* Coupling of T cell receptor specificity to natural killer T cell development by bivalent histone H3 methylation. *J. Exp. Med.* **212**, 297-306 (2015).
86. Kasler, H.G., Lee, I.S., Lim, H.W. & Verdin, E. Histone Deacetylase 7 mediates tissue-specific autoimmunity via control of innate effector function in invariant Natural Killer T Cells. *Elife* **7** (2018).
87. Hirose, S. *et al.* Bcl11b prevents the intrathymic development of innate CD8 T cells in a cell intrinsic manner. *Int. Immunol.* **27**, 205-215 (2015).
88. Gugasyan, R. *et al.* The NF-κB1 transcription factor prevents the intrathymic development of CD8 T cells with memory properties. *EMBO J.* **31**, 692-706 (2012).
89. Godfrey, L. *et al.* DOT1L inhibition reveals a distinct subset of enhancers dependent on H3K79 methylation. *Nat. Comm.* **10**, 2803-2803 (2019).

90. Kerry, J. *et al.* MLL-AF4 Spreading Identifies Binding Sites that Are Distinct from Super-Enhancers and that Govern Sensitivity to DOT1L Inhibition in Leukemia. *Cell Rep.* **18**, 482-495 (2017).
91. Su, I.h. *et al.* Polycomb Group Protein Ezh2 Controls Actin Polymerization and Cell Signaling. *Cell* **121**, 425-436 (2005).
92. Dobenecker, M.W. *et al.* Signaling function of PRC2 is essential for TCR-driven T cell responses. *J. Exp. Med.* **215**, 1101-1113 (2018).
93. Lee, C.-H. *et al.* Automethylation of PRC2 promotes H3K27 methylation and is impaired in H3K27M pediatric glioma. *Genes Dev.* (2019).
94. Bodega, B. *et al.* A cytosolic Ezh1 isoform modulates a PRC2–Ezh1 epigenetic adaptive response in postmitotic cells. *Nat. Struct. Mol. Biol.* **24**, 444-452 (2017).
95. Choi, J. *et al.* DNA binding by PHF1 prolongs PRC2 residence time on chromatin and thereby promotes H3K27 methylation. *Nat. Struct. Mol. Biol.* **24**, 1039-1047 (2017).
96. Lee, C.-H. *et al.* Allosteric activation dictates PRC2 activity independent of its recruitment to chromatin. *Mol. Cell* **70**, 422-422 (2018).
97. Jani, K.S. *et al.* Histone H3 tail binds a unique sensing pocket in EZH2 to activate the PRC2 methyltransferase. *Proc. Natl. Acad. Sci. U.S.A.* **116**, 8295-8300 (2019).
98. Lee, C.-H. *et al.* Distinct Stimulatory Mechanisms Regulate the Catalytic Activity of Polycomb Repressive Complex 2. *Mol. Cell* **70**, 435-448.e435 (2018).
99. Sanulli, S. *et al.* Jarid2 Methylation via the PRC2 Complex Regulates H3K27me3 Deposition during Cell Differentiation. *Mol. Cell* **57**, 769-769 (2015).
100. Soshnev, A.A., Josefowicz, S.Z. & Allis, C.D. Greater Than the Sum of Parts: Complexity of the Dynamic Epigenome. *Mol. Cell* **62**, 681-694 (2016).
101. Chen, S. *et al.* The PZP Domain of AF10 Senses Unmodified H3K27 to Regulate DOT1L-Mediated Methylation of H3K79. *Mol. Cell* **60**, 319-327 (2015).
102. Valencia, A.M. & Kadoch, C. Chromatin regulatory mechanisms and therapeutic opportunities in cancer. *Nat. Cell Biol.* **21**, 152-161 (2019).
103. Feinberg, A.P., Koldobskiy, M.A. & Gondor, A. Epigenetic modulators, modifiers and mediators in cancer aetiology and progression. *Nat. Rev. Genet.* **17**, 284-299 (2016).
104. Cavalli, G. & Heard, E. Advances in epigenetics link genetics to the environment and disease. *Nature* **571**, 489-499 (2019).
105. Berdasco, M. & Esteller, M. Clinical epigenetics: seizing opportunities for translation. *Nat. Rev. Genet.* **20**, 109-127 (2019).
106. Skarnes, W. *et al.* A conditional knockout resource for the genome-wide study of mouse gene function. *Nature* **474**, 337-342 (2011).
107. Carow, B., Gao, Y., Coquet, J., Reilly, M. & Rottenberg, M.E. lck-Driven Cre Expression Alters T Cell Development in the Thymus and the Frequencies and Functions of Peripheral T Cell Subsets. *J. Immunol.* **197**, 2261-2268 (2016).
108. Daniels, M.A. & Jameson, S.C. Critical role for CD8 in T cell receptor binding and activation by peptide/major histocompatibility complex multimers. *J. Exp. Med.* **191**, 335-346 (2000).
109. Frederiks, F. *et al.* Nonprocessive methylation by Dot1 leads to functional redundancy of histone H3K79 methylation states. *Nat. Struct. Mol. Biol.* **15**, 550-557 (2008).

Figure legends

Figure 1: Ablation of *Dot1L* results in $CD44^+CD62L^+$ memory-like $CD8^+$ T cells

a) Analysis of $CD8^+$ T cell subsets in the spleen based on CD44 and CD62L expression in WT and heterozygous and homozygous *Dot1L*-KO mice. Subsets are indicated in the top left panel. b) Quantification of $CD8^+$ T cell subsets in the spleen indicated in the representative plots in panel a. Data from 3-5 individual experiments with 3-4 mice per genotype per experiment, shown as mean ±SD. c) RNA-Seq analysis of sorted $CD44^+CD62L^+$ (T_{CM}) and $CD44^-CD62L^+$ (T_N) $CD8^+$ T cells from four mice per indicated genotype. Naïve and memory signatures were defined based on differentially expressed genes (FDR < 0.01) between WT T_N and WT T_{CM} cells. d) Percentage of $CD49d^+$ cells in $CD44^+CD62L^+$ $CD8^+$ T cells from unchallenged mice and in $CD44^+CD62L^-$ $CD8^+$ T cells from WT mice challenged with L. monocytogenes for 7 days. Data from one experiment with four mice per genotype, represented as mean ±SD. e) Representative flow-cytometry plots of T-bet and EOMES expression in $CD8^+$ T cells from the spleen. f) Median fluorescence intensity of T-bet and EOMES in $CD44^+CD62L^+$ $CD8^+$ T cells from the spleen. Data from one experiment with three mice per genotype, represented as mean ±SD.

Figure 2: The T_{AIM} phenotype in *Dot1L* KO initiates in the thymus and is cell-intrinsic

a) MA-plot of RNA-Seq data from sorted $CD4^-CD8^+CD3^+$ thymocytes from three WT and four KO mice. Naïve and memory signature genes were defined as described in Fig. 1C. b) Representative plot and c) quantification of T-bet and EOMES expression on $CD4^-CD8^+CD3^+$ thymocytes, data of two individual experiments with three mice per genotype, represented as mean ±SD. d-e) Representative plots and quantification of iNKT (CD1d-PBS57$^+$TCRβ$^+$) cells in total thymus. Data from one experiment with four mice per genotype, represented as mean ±SD. f) Absolute number of γδTCR$^+$ cells in spleen, data of two

individual experiments with four mice per genotype, represented as mean ±SD. g) Representative plot of CD44 and CD62L expression on $CD8^+$ T cells in *Lck*-Cre;*Dot1L;OT-I* mice.

Figure 3: *Dot1L* ablation impairs TCR/CD3 expression

a) RNA expression of TCR signaling genes, defined by differential expression between WT and *Dot1L*-KO, in any of the sorted $CD4^-CD8^+CD3^+$ thymocytes (thymus), $CD44^-CD62L^+$ (naïve) $CD8^+$ T cells and $CD44^+CD62L^+$ (memory) $CD8^+$ T cells, four mice per genotype except for WT thymus where there are three mice. Genes are clustered based on z-score. Arrows indicate genes involved in the TCR complex and Itk. Z-score is calculated row-wise within genes between samples. b) Expression of TCRβ, CD3e, TCRα V2, TCRβ V5, CD8α and CD8β on $CD8^+$ T cells in spleen from *Lck*-Cre*;Dot1L* and *Lck*-Cre*;Dot1L;OT-I* mice. c) Absolute number of $CD4^-CD8^+CD3^+$ thymocytes in WT and KO mice from *Lck*-Cre*;Dot1L;OT-I* background, data from two individual experiments with 3-4 mice per genotype, represented as mean ±SD. d) Representative plot and quantification of TCRα V2 and TCRβ V5 expression on $CD8^+$ T cells from spleen. Data from two experiments with 2-4 mice per genotype, represented as mean ±SD.

Figure 4: *Dot1L*-KO T_{AIM} cells have an impaired immune response in vitro and in vivo

a) Analysis of proliferation of CFSE-labeled WT and *Dot1L*-KO $CD8^+$ T cells stimulated with α-CD3/ α-CD28 in vitro. b) IFNγ production by $CD8^+$ T cells after stimulation with α-CD3/α-CD28 for 3 days and Golgi-plug incubation for four hours. c) Outline of immune challenge experiment. On day 0 mice were injected intravenously with a sub-lethal dose of *L. monocytogenes*. Blood was taken at day -3, day 4 and day 7 past injection. At day 3 and 7 past injection mice were sacrificed and spleen and liver were isolated for analysis. On day 3 five mice per genotype were sacrificed, on day 7 3-5 mice per genotype. d) Percentage of CD44 CD62L subsets of $CD8^+$ T cells in blood. e-f) Clearance of *L. monocytogenes* in spleen and liver defined by the number of colony forming units (CFU) per organ. Bars indicate median. g)

Percentage of CD44 CD62L subsets in $CD8^+$ T cells from spleen at day 3 and h) day 7. i) absolute number of $CD3^+CD8^+$ T cells in spleen at day 3 and day 7. j) Intracellular Ki67 positive cells in $CD8^+$ splenocytes. k) Percentage of $KLRG1^+$ in $CD8^+$ T cells from the spleen. l) Percentage of IFNγ-producing cells in $CD8^+$ T cells from spleen after four hours stimulation with PMA/Ionomycin. g-l) Data is represented as mean ±SD.

Figure 5: DOT1L is required for maintenance of the epigenetic identity of $CD8^+$ T cells

a) MA plot indicating differentially expressed genes between *Dot1L* KO and WT in sorted $CD44^-CD62L^+$ (naïve) $CD8^+$ T cells and $CD44^+CD62L^+$ (memory) $CD8^+$ T cells (left). Genes significantly upregulated (red) and downregulated (black) in Dot1L-KO are indicated. Genes were considered differentially expressed when FDR <0.01. Genes outside the limit of the y-axis are indicated with triangles. Right panel shows H3K79me2 normalized read counts of these genes. Genes with low H3K79me2 read counts are blue, genes with high H3K79me2 are red. b) MA plot of gene expression between WT and Dot1L-KO memory $CD8^+$ T cells, with genes differential between activated WT and activated *Ezh2*-KO $CD8^+$ T cells indicated in orange (derepressed in *Ezh2* KO) and blue (downregulated in *Ezh2* KO). Box plot notes effect size in *Dot1L* KO vs WT RNA-Seq data based on the indicated differential gene expression category in *Ezh2* KO data. c) H3K4me3, H3K79me2 and H3K27me3 ChIP-Seq data around transcription start sites from genes that are upregulated in Dot1L KO (KO Gain) and genes that did not change expression (Expression Matched). Coverage was calculated as reads per genomic content, cutoff at the 0.995^{th} quantile and rescaled to a maximum of 1.

Figure 1

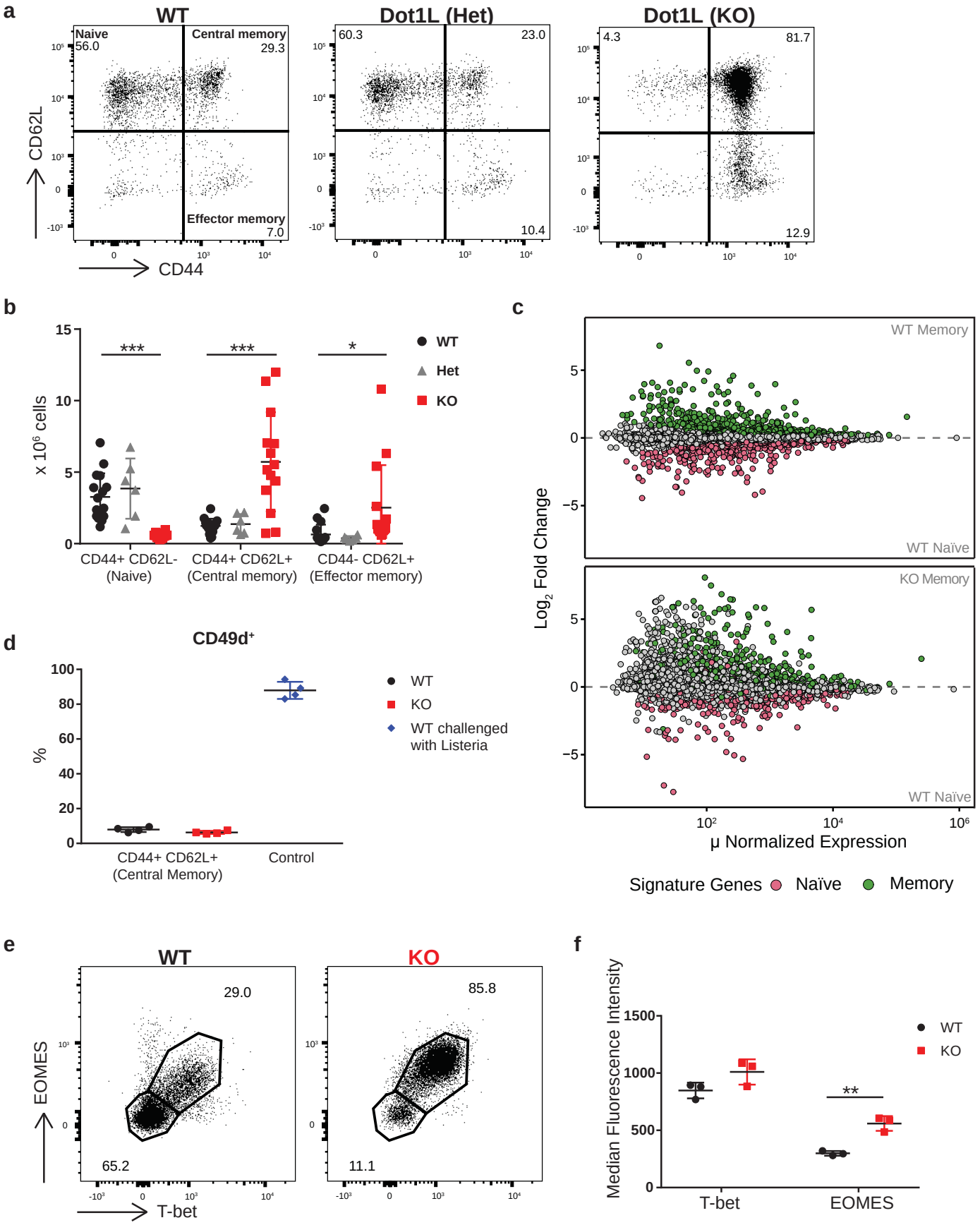
a
WT
Dot1L (Het)
Dot1L (KO)
Naive
56.0
Central memory
29.3
Effector memory
7.0
60.3
23.0
10.4
4.3
81.7
12.9
CD62L
CD44
b
x 10⁶ cells
***
***
*
WT
Het
KO
CD44+ CD62L- (Naive)
CD44+ CD62L+ (Central memory)
CD44- CD62L+ (Effector memory)
c
WT Memory
WT Naïve
KO Memory
WT Naïve
Log2 Fold Change
μ Normalized Expression
Signature Genes
Naïve
Memory
d
CD49d+
%
WT
KO
WT challenged with Listeria
CD44+ CD62L+ (Central Memory)
Control
e
WT
KO
29.0
65.2
85.8
11.1
EOMES
T-bet
f
Median Fluorescence Intensity
WT
KO
**
T-bet
EOMES

Figure 2

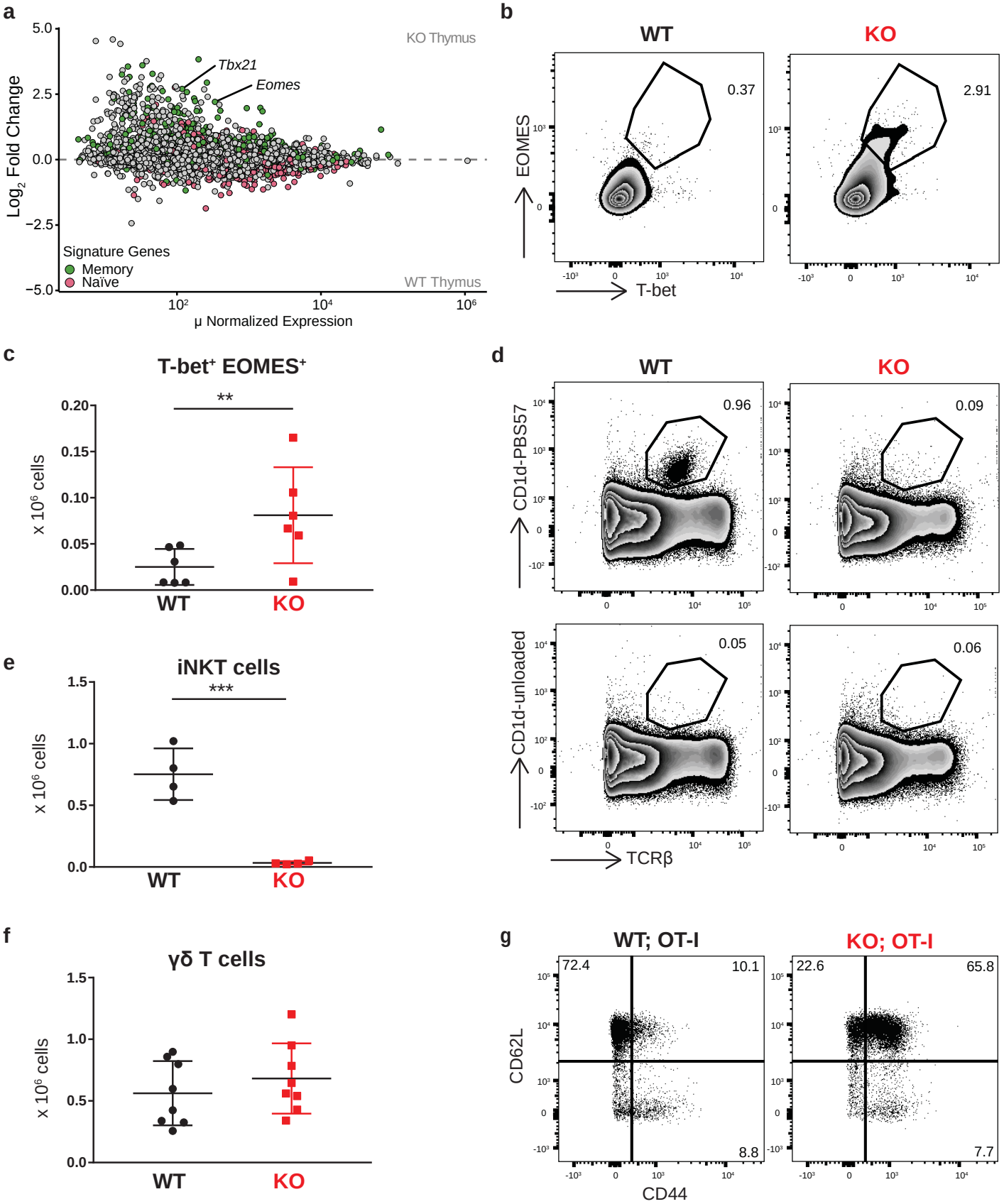
a
KO Thymus
WT Thymus
Tbx21
Eomes
Log2 Fold Change
μ Normalized Expression
Signature Genes
Memory
Naïve
b
WT
KO
0.37
2.91
EOMES
T-bet
c
T-bet+ EOMES+
**
x 10^6 cells
WT
KO
d
WT
KO
0.96
0.09
0.05
0.06
CD1d-PBS57
CD1d-unloaded
TCRβ
e
iNKT cells
***
x 10^6 cells
WT
KO
f
γδ T cells
x 10^6 cells
WT
KO
g
WT; OT-I
KO; OT-I
72.4
10.1
8.8
22.6
65.8
7.7
CD62L
CD44

Figure 3

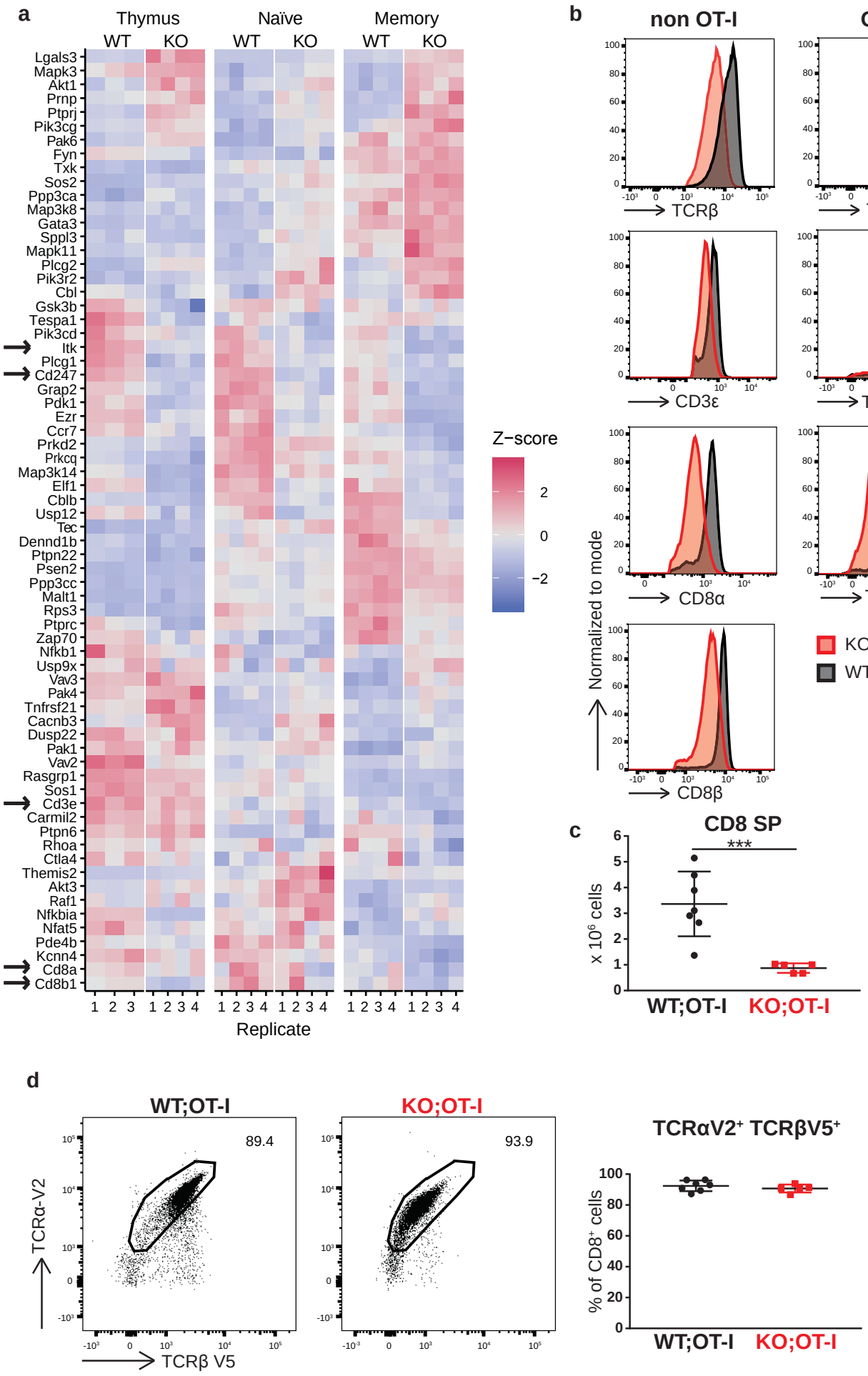
a
Thymus
Naïve
Memory
WT
KO
Lgals3
Mapk3
Akt1
Prnp
Ptprj
Pik3cg
Pak6
Fyn
Txk
Sos2
Ppp3ca
Map3k8
Gata3
Sppl3
Mapk11
Plcg2
Pik3r2
Cbl
Gsk3b
Tespa1
Pik3cd
Itk
Plcg1
Cd247
Grap2
Pdk1
Ezr
Ccr7
Prkd2
Prkcq
Map3k14
Elf1
Cblb
Usp12
Tec
Dennd1b
Ptpn22
Psen2
Ppp3cc
Malt1
Rps3
Ptprc
Zap70
Nfkb1
Usp9x
Vav3
Pak4
Tnfrsf21
Cacnb3
Dusp22
Pak1
Vav2
Rasgrp1
Sos1
Cd3e
Carmil2
Ptpn6
Rhoa
Ctla4
Themis2
Akt3
Raf1
Nfkbia
Nfat5
Pde4b
Kcnn4
Cd8a
Cd8b1
1 2 3 1 2 3 4 1 2 3 4 1 2 3 4 1 2 3 4
Replicate
Z−score
2
0
−2
b
non OT-I
OT-I
TCRβ
CD3ε
TCRα V2
CD8α
TCRβ V5
CD8β
Normalized to mode
KO
WT
c
CD8 SP
***
x 10⁶ cells
WT;OT-I
KO;OT-I
d
WT;OT-I
KO;OT-I
89.4
93.9
TCRα-V2
TCRβ V5
TCRαV2⁺ TCRβV5⁺
% of CD8⁺ cells
WT;OT-I
KO;OT-I

Figure 4

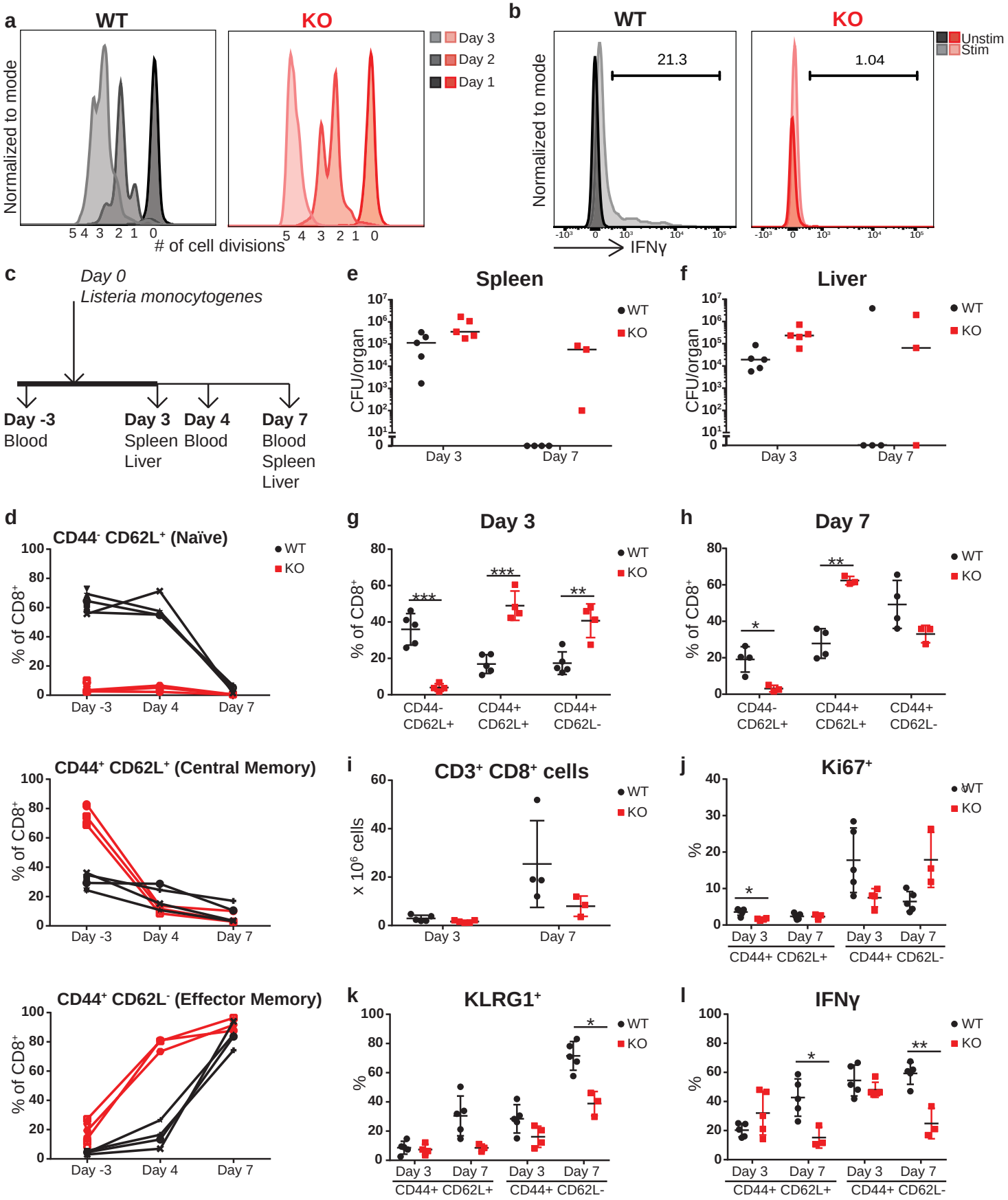
a
WT
KO
Day 3
Day 2
Day 1
Normalized to mode
5 4 3 2 1 0
# of cell divisions
b
WT
KO
Unstim
Stim
21.3
1.04
Normalized to mode
IFNγ
c
Day 0
Listeria monocytogenes
Day -3
Blood
Day 3
Spleen
Liver
Day 4
Blood
Day 7
Blood
Spleen
Liver
e
Spleen
CFU/organ
WT
KO
Day 3
Day 7
f
Liver
CFU/organ
WT
KO
Day 3
Day 7
d
CD44- CD62L+ (Naïve)
% of CD8+
WT
KO
Day -3
Day 4
Day 7
CD44+ CD62L+ (Central Memory)
% of CD8+
Day -3
Day 4
Day 7
CD44+ CD62L- (Effector Memory)
% of CD8+
Day -3
Day 4
Day 7
g
Day 3
% of CD8+
WT
KO
CD44- CD62L+
CD44+ CD62L+
CD44+ CD62L-
h
Day 7
% of CD8+
WT
KO
CD44- CD62L+
CD44+ CD62L+
CD44+ CD62L-
i
CD3+ CD8+ cells
x 10^6 cells
WT
KO
Day 3
Day 7
j
Ki67+
%
WT
KO
Day 3
Day 7
Day 3
Day 7
CD44+ CD62L+
CD44+ CD62L-
k
KLRG1+
%
WT
KO
Day 3
Day 7
Day 3
Day 7
CD44+ CD62L+
CD44+ CD62L-
l
IFNγ
%
WT
KO
Day 3
Day 7
Day 3
Day 7
CD44+ CD62L+
CD44+ CD62L-

Figure 5

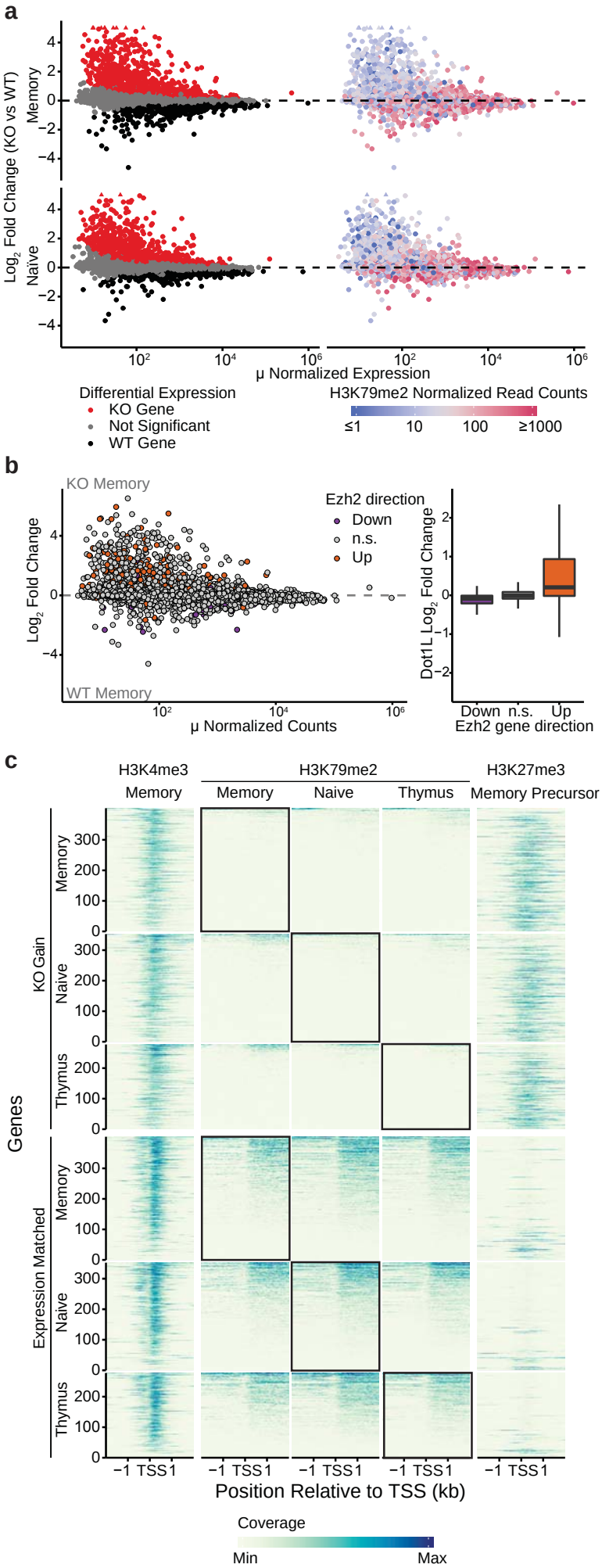
a
Log2 Fold Change (KO vs WT)
Memory
Naïve
μ Normalized Expression
Differential Expression
KO Gene
Not Significant
WT Gene
H3K79me2 Normalized Read Counts
≤1
10
100
≥1000
b
KO Memory
WT Memory
Log2 Fold Change
μ Normalized Counts
Ezh2 direction
Down
n.s.
Up
Dot1L Log2 Fold Change
Down n.s. Up
Ezh2 gene direction
c
H3K4me3
H3K79me2
H3K27me3
Memory
Memory
Naive
Thymus
Memory Precursor
Genes
KO Gain
Expression Matched
Memory
Naive
Thymus
−1 TSS 1
Position Relative to TSS (kb)
Coverage
Min
Max

Table 1: List of candidate negative regulators affected by DOT1L in T cells

Gene	Transcriptional regulator
Hif1a	yes
Srebf2	yes
Lef1	yes
Notch1	yes
Mbd2	yes
Ezr	no
Zeb1	yes
Usp3	yes
Satb1	yes
Fnip1	no
Phb	no
Ezh2	yes
Zbtb20	yes
Rps14	no
Ybx1	yes
Smad7	no
Rpl10	no
Smad4	no
Gatad2a	yes

Ski	no
Etv3	yes
Foxk1	yes

Table 2: Antibodies for surface stains

Antibody	Fluorescent label	Clone	Company
CD3e	APC	145-2C11	BD
CD3e	AF488	145-2C11	eBioscience
TCRβ	PB	H57-597	BioLegend
TCRβ	PE	H57-597	BD
CD4	APC	RM4-5	BioLegend
CD4	BV785	GK1.5	BioLegend
CD8a	BV510	53-6.7	BioLegend
CD8b	PerCpCy5.5	YTS1567.7.7	BioLegend
CD19	APC-H7	1D3	BD
CD19	PE	1D3	BD
CD25	APC	PC61	BioLegend
CD49d	AF488	R-12	BioLegend
CD44	APC-Cy7	IM7	BioLegend
CD44	BV650	IM7	BioLegend
CD45	PerCpCy5.5	30-F11	BioLegend
CD62L	PE	MEL-14	BD
CD62L	PE-Cy7	MEL-14	BioLegend
CD62L	FITC	MEL-14	BD Pharmingen/eBioscience
CD69	PE	H1.2F3	BD
CD90.2	FITC	53-2.1	BD
KLRG1	BV421	2F1/KLRG1	BioLegend

γδTCR	BV605	GL3	BioLegend
TCRαV2	PE	B20.1	BD
TCRβV5	APC	MR9-4	eBioscience
OT-I tetramer	PE	NA	Schumacher group
CD1d tetramer (1:100)	AF488	NA	NIH Tetramer Core Facility
LIVE/DEAD Fixable Near-IR Dead Cell Stain Kit	NA	NA	Thermo Fisher
Zombie NIR	NA	NA	BioLegend
Zombie Violet	NA	NA	BioLegend

Table 3: Antibodies for intracellular stains

Antibody	Fluorescent label	Clone	Company
IFNγ	PE	XMG1.2	BD
T-bet	PE-Cy7	4B10	eBioscience
EOMES	AF488	Dan11mag	eBioscience
EOMES	eF450	Dan11mag	eBioscience
IFNγ	PE-Cy7	XMG1.2	eBioscience
Ki67	PE	SolA15	eBioscience

Table 4: Antibodies for cell sorting

Antibody	Fluorescent label	Clone	Company
CD3	AF488	145-2C11	eBioscience
CD4	APC	RM4-5	BioLegend
CD8	PerCp-Cy5.5	YTS1567.7.7	BioLegend
CD44	APC-Cy7	IM7	BioLegend
CD62L	PE	MEL-14	BD biosciences
TCRβ	PE	H57-597	BD